CIAiS

Research and Education Consortium
for Innovation of Advanced Integrated Science

INTERNATIONAL SYMPOSIUM 2019

THE UNIVERSITY OF TOKYO

Keio University

WASEDA University

Tokyo Institute of Technology

UEC TOKYO

CIAiS

Friday, March 1 13:30-19:00
Fukutake Hall, The University of Tokyo

Welcome Address

On behalf of the Research and Education Consortium for Innovation of Advanced Integrated Science (CIAiS), I would like to welcome all of you to the 2019 CIAiS International Symposium.

CIAiS is a cooperative effort between The University of Tokyo, Keio University, Waseda University, Tokyo Institute of Technology, and The University of Electro-Communications. Its partners are the National Institute for Materials Science (NIMS), RIKEN, and Kawasaki City. CIAiS began as a result of research produced by the Academic Consortium for Nano- and Micro-Fabrication, conducted through collaboration between the Four University Research Institute and the Advanced Photon Science Alliance (APSA). CIAiS brings together researchers from a wide range of fields to conduct new, high-quality, interdisciplinary research.

A stable, yet highly mobile employment system is used within the Consortium, in place of a more traditional short-term employment system where individuals are separated by institutions and departments. This is made possible as a result of budget provisions and an equalized system that transcends organizations. Next-generation researchers can engage in work while also considering career advancement. The Consortium provides post-docs and doctoral students with a variety of educational programs to facilitate experiences in different fields of study, help students develop a more comprehensive outlook, and to produce human resources who can work in diverse environments. We must encourage individuals who can innovate on a global scale. It is through these efforts that the Consortium aims to present researchers with career path models and increase the number of young people who would like to become researchers.

This symposium will give an overview of research efforts and will introduce the next-generation researchers at CIAiS. I hope the symposium will be a wonderful experience for all participants, and that it serves as an opportunity for new networks and research collaborations to begin.

Shigeo Maruyama
CIAiS Consortium Director
Professor, Department of Mechanical Engineering,
School of Engineering, The University of Tokyo

CIAiS International Symposium 2019

Table of Contents

CIAiS International Symposium 2019

Research and Education Consortium for Innovation of Advanced Integrated Science

Friday, March 1, 2019 13:30-19:00

Fukutake Hall, The University of Tokyo

13:00 **Poster Open**

Opening 13:30-13:50

Chair: Yuta Yoshimoto

13:30-13:50 **Welcome Address**

Shigeo Maruyama

Consortium Director, The University of Tokyo

Opening Address

Keiji Yamamoto

Program Officer, Japan Science and Technology Agency

Keynotes 13:50-15:05

Chair: *Il Jeon, Tomotake Yamakoshi, Yasushi Shinohara, Xiao-Mei Zhang*

13:50-14:20 **Wafer-Scale Crystalline Carbon Nanotube Films**

Junichiro Kono

Department of Electrical and Computer Engineering,
Department of Physics and Astronomy,
Department of Materials Science and Nano Engineering, Rice University

14:20-14:35 **Hybrid graphene/metal reflectarray for THz communications**

Erik Einarsson

Department of Electrical Engineering
Department of Materials Design and Innovation
The State University of New York, University at Buffalo

14:35-14:50 **Direct FC-CVD synthesis of Colorful and Conductive SWNT thin films**

Esko I. Kauppinen

School of Science
Department of Applied Physics, Aalto University

14:50-15:05 **Selective Synthesis of Single-Walled Carbon Nanotubes**

Yan Li

College of Chemistry and Molecular Engineering, Peking University

15:05-15:15 Break

Poster Presentation 15:15-15:50

Chair: Tomotake Yamakoshi, Yasushi Shinohara

15:15-15:50 Poster 1 min Presentation

Next-generation Researchers 15:50-16:50

Chair: *Yasushi Shinohara, Il Jeon, Xiao-Mei Zhang, Tomotake Yamakoshi*

15:50-16:05 **Solution-Processed Double-walled Carbon Nanotube Transparent Electrode for Perovskite Solar Cells**
Il Jeon
Department of Mechanical Engineering, School of Engineering,
The University of Tokyo

16:05-16:20 **Thickness Optimization of Porous Silicon and Surface Passivation via Formation of Anodic SiO2 for Solar Cells Application**
Xiao-Mei Zhang
Department of Chemical Science and Engineering; Department of Mechanical Engineering, Tokyo Institute of Technology

16:20-16:35 **Coherent manipulation of ultracold atoms in optical lattices**
Tomotake Yamakoshi
Institute for Laser Science, University of Electro-Communications

16:35-16:50 **Theoretical Study of Electron Dynamics under Intense Laser Field: Effects of Spatial Variation and Polarization of the Field**
Yasushi Shinohara
Photon Science Center, School of Engineering, The University of Tokyo

Closing 16:50-17:00

Chair: *Yuta Yoshimoto*

16:50-17:00 **Closing Remarks**
Koichi Hishida
Department of System Design Engineering, Keio University

Poster Session 17:00-17:30

Chair: Xiao-Mei Zhang, Il Jeon

17:00-17:30 Poster Session

Social Gathering 17:30-19:00

Chair: *Tomotake Yamakoshi, Yasushi Shinohara*

17:30-19:00 Social Gathering
CIAiS Poster Awards

Keynotes

Wafer-Scale Crystalline Carbon Nanotube Films

Junichiro Kono
Department of Electrical & Computer Engineering, Department of Physics & Astronomy, and
Department of Materials Science & NanoEngineering, Rice University
kono@rice.edu

We have recently developed a controlled vacuum filtration method for the preparation of wafer-scale films of crystalline chirality-enriched single-wall carbon nanotubes [1,2]. This talk will first describe the controlled vacuum filtration technique [2] and then summarize our recent discoveries in optical spectroscopy studies and optoelectronic device applications using films prepared by this technique. These include the observation of intersubband plasmons [3], microcavity exciton polaritons with polarization-dependent ultrastrong coupling [4], isotropic Seebeck coefficient with anisotropic electrical conductivity [5], and the direct observation of cross-polarized excitons [6].

1. For a review, see, e.g., W. Gao and J. Kono, arXiv:1810.02928.
2. X. He *et al*., Nature Nanotechnology **11**, 633 (2016).
3. K. Yanagi *et al*., Nature Communications **9**, 1121 (2018).
4. W. Gao *et al*., Nature Photonics **12**, 362 (2018).
5. K. Fukuhara *et al*., Applied Physics Letters **113**, 243105 (2018).
6. F. Katsutani *et al*., Physical Review B **99**, 035426 (2019).

Hybrid graphene/metal reflectarray for THz communications

Erik Einarsson
Department of Electrical Engineering, Department of Materials Design and Innovation,
University at Buffalo
erikeina@buffalo.edu

Our collective desire for ever-faster communications has driven technological advances, resulting in a doubling of wireless data rates approximately every 18 months [1]. This trend, known as Edholm's law of bandwidth, predicts Terabit-per-second (Tbps) data rates within a few short years. This presents a considerable hurdle, as existing technologies cannot support such high-speed operation. New approaches incorporating novel materials are required to access the currently unutilized terahertz band [2].

The major challenge to operating in the THz band (0.1 THz to 10 THz) is significant path loss that is primarily due to absorption by water vapor in the atmosphere. Improving THz sources and detectors is one way to overcome this problem, and there have been considerable advances in recent years [3, 4]. In addition to increased detector sensitivity and emitter power, directional antenna arrays are necessary to concentrate and steer the transmitted signals. Consequently, there is a critical need for compact antenna arrays capable of transmitting and receiving information in the THz band. In order to achieve this goal, control of the array response is essential. Toward this end, we report fabrication and characterization of a hybrid graphene/metal antenna array consisting of metallic elements fabricated atop a monolayer graphene sheet. The Fermi energy of graphene can be easily tuned by electrostatic gating, making this graphene/metal hybrid structure an important step toward steerable THz reflectarrays.

We grew graphene on copper foil by chemical vapor deposition [5] at 1000 °C using methane as a carbon source. We transferred the resulting graphene using a combination of poly(methyl methacrylate) (PMMA) and a compatible copolymer [6] onto a silicon substrate. After transfer, we patterned gold antennas atop the graphene using electron-beam lithography. Antenna dimensions and spacing were determined by COMSOL Multiphysics simulations. Graphene parameters used in the simulations were determined from the complex conductivity, which we extracted using time-domain terahertz spectroscopy [7]. An optical image of the fabricated reflectarray is shown in Fig. 1a, and a simulation of the electric field response is inset.

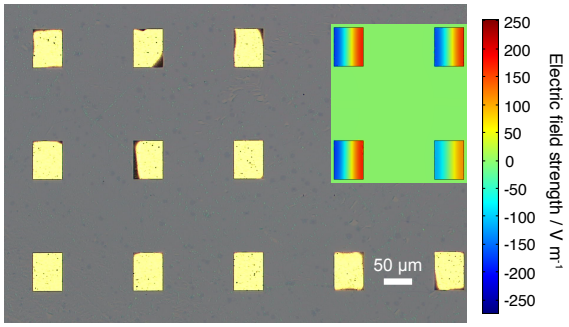

(a) Optical micrograph of an array of gold antennas fabricated atop graphene. Inset shows COMSOL simulation of electric field response in a 2×2 antenna array.

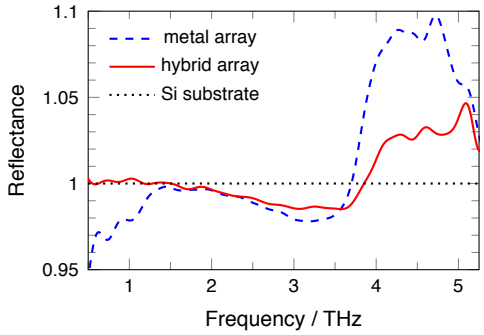

(b) THz reflectance relative to the underlying substrate. Increased reflectance by the array is apparent at 4.5 THz and is weakened by the presence of graphene.

Figure 1: Fabricated and characterized hybrid graphene/metal reflectarray

In Figure 1b we plot the response of the graphene/metal hybrid antenna array, as well as a metal array with identical dimensions but no underlying graphene. Reflectance is calculated relative to the underlying substrate reference, thus a value larger than unity corresponds to enhanced reflection by the array. The array elements were designed to resonate near 1.5 THz. While we observe no change at 1.5 THz, the reflectance is clearly enhanced at 4.5 THz, corresponding to resonance at $3\lambda/2$. The decrease in reflectance when graphene is present can be understood by considering that, while it is a good conductor, graphene typically has a small density of states at the Fermi level. Having graphene on the surface under the array softens the electronic boundary condition at each element, making them slightly "leaky." The result is suppressed reflection at the boundary and reduced overall reflected power. This is advantageous because it facilitates modulation of the array response because the Fermi energy of graphene—and by extension the charge carrier concentration and electrical conductivity—can be tuned by electrostatic gating. The effect of such modulation would soften or sharpen the boundary, thereby changing the plasmon reflection from the edges and, consequently, the reflected power.

[1]S. Cherry, "Edholm's law of bandwidth", IEEE Spectrum **41**, 58–60 (2004).

[2]I. F. Akyildiz and J. M. Jornet, "The internet of nano-things", IEEE Wireless Communications (2010).

[3]R. Bogue, "Sensing with terahertz radiation: a review of recent progress", Sensor Review **38**, 216–222 (2018).

[4]W. Xu, L. Xie, and Y. Ying, "Mechanisms and applications of terahertz metamaterial sensing: a review", Nanoscale **9**, 13864–13878 (2017).

[5]X. Li et al., "Large-area synthesis of high-quality and uniform graphene films on copper foils", Science **324**, 1312–1314 (2009).

[6]A. Karmakar et al., "Approaching completely continuous centimeter-scale graphene by copolymer-assisted transfer", RSC Adv. **8**, 1725–1729 (2018).

[7]Y. Zhou et al., "Terahertz wave reflection impedance matching properties of graphene layers at oblique incidence", Carbon **96**, 1129–1137 (2016).

Direct FC-CVD synthesis of Colorful and Conductive SWNT thin films

Esko I. Kauppinen

Author Aalto University School of Science, Department of Applied Physics

PO Box 15100, FI-00076 Aalto, FINLAND

esko.kauppinen@aalto.fi

We have explored floating catalyst chemical vapor deposition (FC-CVD) synthesis of single walled carbon nanotubes (SWNT) via tuning tube atomic structure i.e. (n,m) distributions. Ferrocene has been used as the catalyst nanoparticle precursor and CO, C_2H_4 and ethanol as the carbon precursors, with CO_2, H_2O and H_2S as the respective additives to tune (n,m) distributions. By introducing various amount of CO_2 in FC-CVD with CO as the carbon source and in-situ ferrocene decomposition generated Fe catalyst nanoparticles, we directly synthesized SWNT films with tunable (n,m) i.e. helicity distribution as well as tunable colors [1]. When operating the FC-CVD reactor at the ambient pressure and at 850 ºC temperature with 0.25 and 0.37 volume percent of added CO_2, the SWNT films display green and brown colors, respectively. We ascribed various colors to suitable diameter and narrow (n,m) distributions, which were determined in detail using the electron diffraction. We will present recent results on using ethylene as the carbon source in nitrogen carrier gas with the addition of H_2O vapor to synthesize SWNTs with extremely narrow (n,m) distribution and directly deposit colorful films. Finally, we present results to simulate the observed film colors based on experimentally determined (n,m) distributions of tubes and their light absorption functions.

References

[1] Y. Liao et al." Direct Synthesis of Colorful Single-Walled Carbon Nanotube Thin Films". *J. Am. Chem. Soc.* **140**, 31, 9797-9800 (2018).

Selective Synthesis of Single-Walled Carbon Nanotubes

Yan Li

College of Chemistry and Molecular Engineering, Peking University, Beijing 100871, China.

Department of Mechanical Engineering, The University of Tokyo

Email: yanli@pku.edu.cn

Single-walled carbon nanotubes (SWNTs) have shown great potentials in various fields attributing to their unique structure-dependent properties, therefore, the structure-controlled preparation of SWNTs is a crucial issue for their advanced applications (e.g. carbon-based nanoelectronics) and has been a great challenge for about two decades. We developed a strategy to produce SWNTs with specific chirality by using a new family of catalysts, tungsten-based intermetallic compound nanocrystals. This kind of catalysts can maintain their unique atomic arrangements during chemical vapor deposition process to regulate the chirality of the grown SWNTs. Using W_6Co_7 as catalysts, (12,6), (14, 4), and (16,0) SWNTs with high purity were directly synthesized under optimized condition. This can be a general strategy for structure-specified growth of SWNTs.

Next-generation Researchers

Solution-Processed Double-walled Carbon Nanotube Transparent Electrode for Perovskite Solar Cells

Il Jeon

Department of Mechanical Engineering, The University of Tokyo

il.jeon@spc.oxon.org

Over the last 20 years, carbon nanotubes (CNTs) have generated a great deal of excitement among researchers for their applicability in electronics. In addition to high conductivity, CNTs films demonstrate high transparency with remarkable mechanical resilience. Accordingly, they have been regarded as a promising alternative to conventional electrodes such as indium tin oxide (ITO) and metals. Thus far, single-walled CNTs (SWNTs) have frequently been the subject of study for transparent electrode applications. This is because SWNTs possess lower optical density than multi-walled CNTs (MWNTs). However, MWNTs have a unique advantage of being solution-processed. Since other carbon electrodes, such as graphene, and carbon pastes, are not solution-processable, solution-processable CNT electrodes could potentially be the game changer in optoelectronics. Double-walled CNTs (DWNTs), which have a unique two concentric graphitic tubular shape, is structurally intermediate between SWNTs and MWNTs. DWNTs have the best of the both worlds in a way that they exhibit good dispersibility and chemical stability of MWNTs, while demonstrating high transparency and conductivity of SWNTs. In other words, solution-processable CNT can be achieved by using DWNTs, which possess excellent optoelectronic properties yet are chemically, mechanically, and thermally more stable than SWNTs.

In the wake of recent energy crisis, organometallic halide perovskite solar cells (PSCs) have emerged as a promising thin-film photovoltaic with its high power conversion efficiency (PCE) and solution-processability. While high PCE is an eye-catching property at a laboratory level, it is only part of a big picture for industrial applications. In order for PSCs to maximize their potential, it is imperative that their brittle and high-cost ITO – or fluorine-doped tin oxide (FTO) – are replaced by a cost-effective and flexible alternative, such as CNTs. In particular, solution-processable DWNT electrode in PSCs can open up a new revenue towards large-size low-cost PSCs.

In this work, we synthesized narrowly distributed diameters of long DWNTs, and slot-die coated them on substrates. We studied the optoelectronic properties of the films and found that

they showcase higher transparency and conductivity than the previously reported CNT electrodes. Moreover, DWNTs were less susceptible to chemical doping than SWNTs on account of their unique double-walled structure and the surrounding surfactants. The produced DWNT films possessed a permutation of metallic outer walls, and a mixture of semiconducting and metallic inner walls. Inverted-type PSCs were fabricated using DWNT films to demonstrate their potential as the transparent electrodes. The solution-processed DWNT electrode-based PSCs exhibited a PCE of 15.8% before doping, which improved to 16.8% and 17.3% upon HNO_3 and trifluoromethanesulfonic acid (TFMS) doping, respectively. This was comparable to 19% of the ITO-based reference devices.

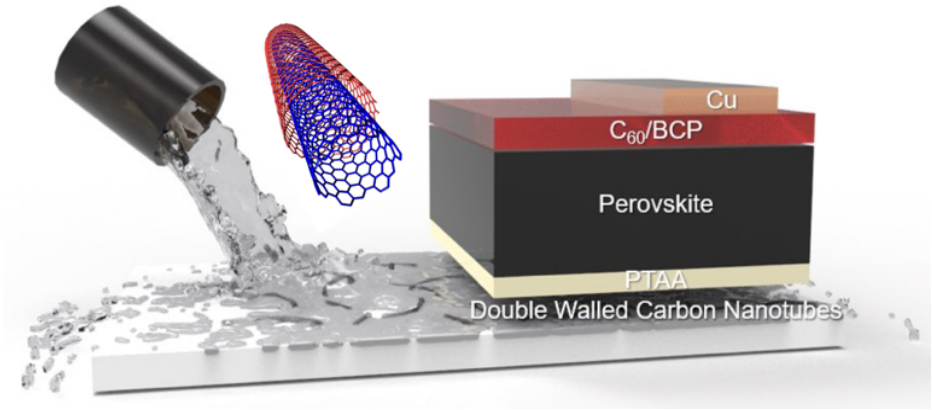

References

[1] Jeon, I. *et al.* Direct and Dry Deposited Single-Walled Carbon Nanotube Films Doped with MoOx as Electron-Blocking Transparent Electrodes for Flexible Organic Solar Cells. *J. Am. Chem. Soc.* **2015**, *137*, 7982-7985. [2] Jeon, I. *et al.* Single-Walled Carbon Nanotube Film as Electrode in Indium-Free Planar Heterojunction Perovskite Solar Cells: Investigation of Electron-Blocking Layers and Dopants. *Nano Lett.* **2015**, *15*, 6665-6671. [3] Jeon, I. *et al.* Carbon Nanotubes versus Graphene as Flexible Transparent Electrodes in Inverted Perovskite Solar Cells. *J. Phys. Chem. Lett.* **2017**, *8*, 5395-5401.

Thickness Optimization of Porous Silicon and Surface Passivation via Formation of Anodic SiO_2 for Solar Cells Application

Xiao-Mei Zhang[1,2], Ryoji Yogai[2], Kazuki Murakami[2], Panus Sundarapua[2], Alain Fave[4], Kei Hasegawa[2], Manabu Ihara[1,3]

[1] Department of Mechanical Engineering; [2] Department of Chemical Science and Engineering; [3] Department of Chemistry, Tokyo Institute of Technology, Tokyo, Japan; [4] Institute des Nanotechnologies de Lyon (INL), France

Email: zhang.x.as@m.titech.ac.jp

Solar cells are an important contribution to renewable energy for fueling our economics. Silicon (Si) is the only material that combines suitable optoelectronic properties with technological availability and abundance. Currently, power conversion efficiency of 26.7% for a single junction Si solar cell can be demonstrated in lab, [1] which is very close to the Shockley-Queisser limit of 30%. [2] The present efficiency and cost of Si solar cells limit the wider application of Si cells. Porous Si (PS) boasts unique properties, including a wide band gap (1.8-2.2 eV), efficient antireflection coatings (ARCs) and wide optical transmission range (700-1000 nm). Due to these unique features, PS is a good candidate for applications as a top absorber in multi-junction Si tandem cells, which combine low- and high-bandgap materials tailored to the incident solar spectrum. It has a theoretical efficiency of 44% for two junction tandem cells. [3]

One of the main challenges that hamper the application of PS in solar cells are related to the increasing recombination due to its large surface area. PS surface passivation is a challenging task due to their miniscule size having aspect ratios as high as 400:1. [4] For phosphorus diffused n^+ emitters of *p*-type solar cells, SiO_2 films can provide good passivation owing to its excellent chemical passivation for the Si-SiO_2 interface. The effect of the thermally grown SiO_2 is limited to PS structures because SiO_2 particles are normally difficult to deposit on deep and narrow pores PS surface with high aspect ratio. Attempts are being made to find another approach to produce high-quality SiO_2 film with low cost. Electrochemical method has been used to fill nanopores in a template with conducting, semiconducting or bio-molecular materials, in order to fabricate nanostructures and integrate them in circuit components [5]. During the anodizing process within an acidic medium, electrode reactions (oxidation and reduction) in combination with field-driven ion diffusion lead to the formation of an oxide layer on the anode (PS) surface.

In this work, we investigate the photovoltaic effect in anodic formation of SiO_2 on a PS surface toward a potential passivation technique for high aspect ratio PS solar cells device application. Three types of PS layers are investigated for improving the efficiency of Si solar cells by varying their thickness from 146 to 545 nm. The PS layers are prepared by electrochemical anodization in a hydrofluoric acid (HF) containing electrolyte. Figure 1 shows the cross-section TEM images of the fabricated Type-1, Type-2, and Type-3 PS layers. They are further constructed to PS solar cells acting as a wide-gap absorber and anti-reflection coatings. SiO_2 passivation layer is electrochemically formed on the PS surface in (HCl: H_2O) solution at room temperature. The dependence of photovoltaic performance including short-circuit current density (J_{sc}), open-circuit voltage (V_{oc}) power conversion efficiency (η), fill-factor (FF), series and shunt resistance is examined in relation to the passivation time. The anodization process using the silicon-on-insulator (SOI) structure provides the advantages of uniform bottom-up passivation along the depth of the PS layer.

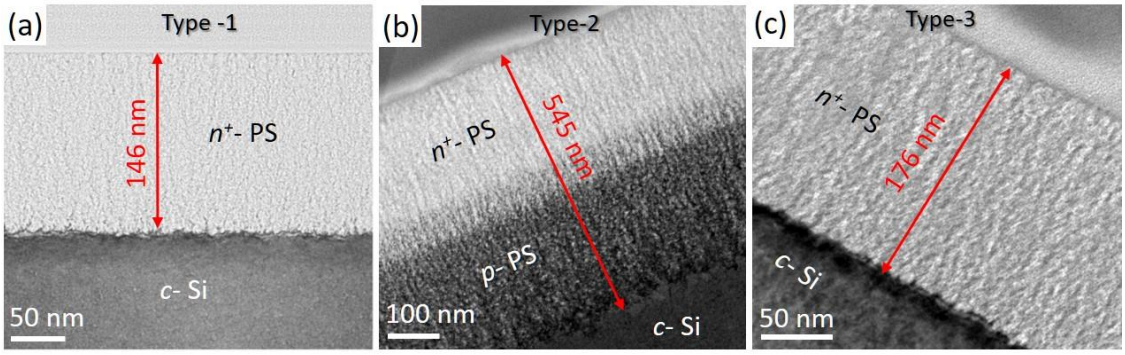

Figure 1. TEM images of the fabricated PS layers. (a) Type-1 PS, (b) Type-2 PS, (C) Type-3 PS.

Acknowledgments

This work was supported by JST in Japan, Research and Education Consortium for Innovation of Advanced Integrated Science (CIAiS).

References

1) K. Yoshikawa *et al*., Silicon heterojunctionsolar cell with interdigitated back contacts for a photoconversion effi-ciency over 26%. Nat. Energy, 2 (5), 17032 (2017).
2) W. Shockley *et al*., Detailed Balance Limit of Efficiency of p‐n Junction Solar Cells. J. Appl. Phys. 32, 510 (1961).
3) A. Martí, *et al*., Limiting efficiencies for photovoltaic energy conversion in multigap systems. Sol. Energy Mater. Sol. Cells, 43, 203 (1996).
4) J. J. Patil *et al*., Ultra-high aspect ratio functional nanoporous silicon via nucleated catalysts. RSC Adv. 7, 11537 (2017).
5) R. W. Berg *et al*. Raman and ab Initio Studies of Simple and Binary 1-Alkyl-3-methylimidazolium Ionic Liquids. J. Phys. Chem. B,109 (40), 19018 (2005).

Coherent manipulation of ultracold atoms in optical lattices

Tomotake Yamakoshi
Institute for Laser Science, University of Electro-Communications
t_yamakoshi@ils.uec.ac.jp

Ultracold atoms and molecules in optical lattices have been eagerly investigated over the last 20 years. These quantum systems are suitable for simulating various Hamiltonian systems in the lattice such as the Hubbard model and recent experiments demonstrated their high controllability and accessibility. In recent years, unconventional phenomena in higher bands have attracted much attention with a view to developing new quantum technologies.

One of the intriguing topics is coherent wave packet preparation of a target state with high fidelity. Especially, coherent population transfer onto a specific band is a prerequisite for achieving coherent quantum control over a wide range of phase space in the optical lattice system. The Aarhus group succeeded in conducting coherent manipulation by using amplitude modulation of the optical lattice[1]. This technique conserves energy and quasimomentum during an interband transition; thus it is suitable for the coherent wave packet shaping and the band spectroscopy although the transfer rate is rather low(~20%). On the other hand, an experimental group in Beijing demonstrated[2] that a similar technique called the "standing-wave pulse sequence" was extremely efficient(~90%). It repeatedly turns the optical lattice on and off and applies time-wise pulses of the impulse to confined ultracold atoms with appropriate time intervals. This technique was applied to promote the wave packet into the fourth excited band with high fidelity to study the dynamics of ultracold atoms in the combination of an optical lattice and a harmonic trap; however, the wave packet is not robust due to the band gap and unharmonic dispersion.

In this talk, we present the numerical results of coherent population transfer by the standing-wave pulse sequence method with a one-dimensional bichromatic optical lattice system for the major purpose of producing dense and robust wave packets. For an ideal set of parameters, the population transfer from the ground band to the first and second excited bands is attained with 90% efficiency. In addition, we demonstrate that the excited wave packet is very robust with appropriate parameters due to an unconventional parabolic dispersion of the bichromatic lattice[3]. The combination of the standing-wave pulse and the amplitude

modulation may pave the way to investigating low-dimensional quantum properties subject to a designed band structure.

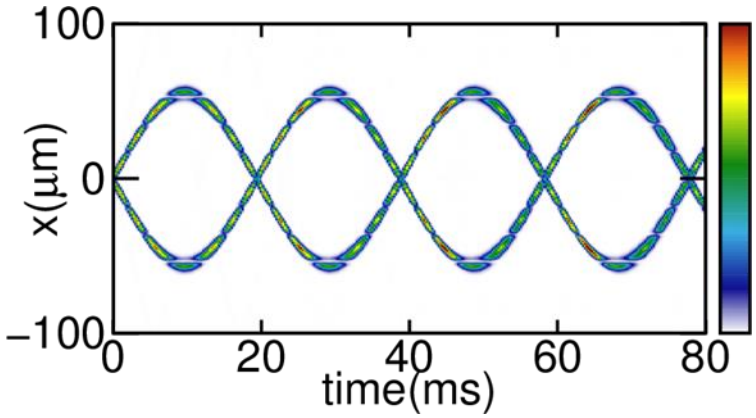

Fig1. Time evolution of stable wave packet in the combined potential of the bichromatic lattice and the harmonic potential.

References

[1] P. L.Pedersen *et al.*, Phys. Rev. A 88, 023620 (2013).

[2] X. Zhou, S. Jin, and J. Schmiedmayer, New J. Phys. 20, 055005(2018).

[3] Tomotake Yamakoshi and Shinichi Watanabe, Phys. Rev. A 99, 013621(2019).

Theoretical Study of Electron Dynamics under Intense Laser Field: Effects of Spatial Variation and Polarization of the Field

Yasushi Shinohara
School of Engineering, The University of Tokyo
shinohara@atto.t.u-tokyo.ac.jp

Recent progress of coherent light source technologies allows us to use a strong light-field whose intensity is comparable to field strength electrons feel in materials. Materials under the strong light field reveal highly nonlinear responses. To obtain microscopic physical pictures and even predict new phenomena in experiments, we have developed theoretical frameworks to describe electron dynamics under such intense light-field.

Fine structures of the light-field can be more enhanced for the electron dynamics driven by the stronger light field because of its nonlinearity. Two examples of the enhancement are a) the coupling between angular momentum and the light magnetic field due to spatial variation of the light-field [1, 2] and b) polarization state of the light affecting on high-order harmonic generation spectra from graphene [3]. We develop two theoretical frameworks along these directions.

An approximation that spatial variation is not taken into account, so-called dipole approximation, has been frequently employed. This approximation is not capable to describe a coupling between angular momentum and light magnetic field which is the leading term to distinguish chirality of materials. There are two gauges, length-gauge and velocity-gauge, to describe electron dynamics under the field within the dipole approximation. A gauge transformation between wave functions in the gauges are well known. A gauge transformation for spatially arbitral light-field is known as Power-Zienau-Woolley transformation [4] as well. However, there are confusions about reliable gauge transformation for approximated light-field shapes based on Taylor expansion of spatial coordinate The gauge transformations are important for theoretical foundation and crucial to perform theoretical simulations. To conclude reliable gauge transformation for the approximated light-field, we develop a theory of gauge transformations for arbitral shape light-field beyond dipole approximation based on the multipole expansion of the field [5].

It has been proposed that theoretical formulae of transition rate of crystalline solids due to the strong light-field, e.g. proposed by Keldysh [6]. This Keldysh-formula just refers to the

effective mass and bang gap as material-specific physical properties. Simplicity to evaluate the transition rate is a beauty for quick trial-and-error cycles in experiments. Most of the simple formulae are for the transition rate under linearly polarized light-field. We develop a theory to evaluate the transition rate under strong circularly polarized light by a simple formula [7].

[1] Yoichi Harada, Eisuke Haraguchi, Keisuke Kaneshima, and Taro Sekikawa, Phys. Rev. A **98**, 021401 (2018).

[2] Denitsa Baykusheva and Hans Jakob Wörner, Phys. Rev. X **8**, 031060 (2018).

[3] Naotaka Yoshikawa, Tomohiro Tamaya, and Koichiro Tanaka, Science **356**, 736 (2017).

[4] Rodney Loudon, "The Quantum Theory of Light", Oxford University Press (1973)

[5] Ryoji Anzaki, Yasushi Shinohara, Takeshi Sato, Kenichi L. Ishikawa, Phys. Rev. A **98** (2018) 063410.

[6] L. V. Keldysh, Sov. Phys. JETP **20**, 1307 (1965).

[7] Tomohito Otobe, Yasushi Shinohara, Shunsuke A. Sato, and Kazuhiro Yabana, J. Phys. Soc. Jpn. **88** (2019) 024706.

Poster Session

Poster List

Poster No,	Name	Institution	Affiliation	Presentation Title	Page
1	Hao-Sheng Lin	The University of Tokyo	Department of Mechanical Engineering	Achieving High Efficiency in Solution-Processed Perovskite Solar Cells using C60/C70 Mixed Fullerenes	20
2	Abhishek Thote	The University of Tokyo	Department of Mechanical Engineering	Stable and Reproducible 2D/3D Formamidinium–Lead–Iodide Perovskite Solar Cells	21
3	Hayato Arai	The University of Tokyo	Department of Mechanical Engineering	Growth of Boron Nitride Layers on Single-Walled Carbon Nanotubes and Graphite	22
4	Ahmed Shawky Mohammed Ghareeb	The University of Tokyo	Department of Mechanical Engineering	Enhancing the Stability of Perovskite Solar Cells via Lithium-ion Endohedral Fullerenes on Top of Laminated Carbon Nanotube Electrodes	23
5	Dong Hyun Yoon	Waseda University	Faculty of Science and Engineering	Oil-in-water droplet formation in hydrophobic PDMS device using three-dimensional protruded taper channel	24
6	Pengyingkai Wang	The University of Tokyo	Department of Mechanical Engineering	Enhanced in-plane thermal conductivity of single-walled carbon nanotube/boron nitride nanotube composite films	25
7	Bunsho Koyano	The University of Tokyo	Department of Mechanical Engineering	Isotope Labelling Analysis for Regrowth of Single-Walled Carbon Nanotubes	26
8	Ryo Soma	Keio University	Graduate School of Science and Technology	Dynamical control of phase-change material coated Janus particles	27
9	Bokusui Nakayama	Keio University	Graduate School of Science and Technology	Dynamics of Colloidal Particles in a Temperature-Responsive Polymer Solution	28
10	Shuhei Okawa	The University of Tokyo	Department of Mechanical Engineering	Polyaromatic Anthracene Clencher on Single-Walled Carbon Nanotubes as Cathodes in Perovskite Solar Cells	29
11	Toshihiro Kaneko	The University of Tokyo	Department of Mechanical Engineering	Quantitative prediction of oxygen diffusion resistance and porous characters under capillary condensation of water in the mesoporous cathode catalyst layer of polymer electrolyte fuel cell	30
12	Eiji Kajikawa	University of Electro-Communications	Institute for Laser Science	MOFA system at around 810 nm with Tm3+-doped ZBLAN fiber	31
13	Rei Sakakibara	The University of Tokyo	Department of Applied Physics	Coherent polarization beam combination for the light source of KAGRA	32
14	Seren Maeda	Waseda University	School of Fundamental Science and Engineering	Water-Electrokinetic Energy Harvester using Flexible Woody Carbon Film	33
15	Kaoru Hisama	The University of Tokyo	Department of Mechanical Engineering	Energetics and electronic structure of single walled carbon nanotube encapsulated in boron nitride nanotube	34
16	Takuma Teramura	The University of Tokyo	Department of Nuclear Engineering and Management	Gauge-Invariant Time-Dependent Configuration Interaction Singles Method for Multielectron Dynamics under Intense Laser Field	35
17	Kenta Sasagawa	Waseda Universit	Department of Nanoscience and Nanoengineering	Low Cost and High-Efficient Piezoelectric MEMS Energy Harvester with Interdigitated Electrodes and Liquid-based VDF-TrFE	36
18	Mizuki Tani	The University of Tokyo	Department of Systems Innovation	Theoretical study on inter-atomic distance effects on high-order harmonic generation	37
19	Keiichiro Toda	The University of Tokyo	Department of Physics	Molecular contrast added to phase-contrast microscope	38
20	Hiroyuki Tahara	The University of Tokyo	Department of Applied Physics	Development of an Auto-Alignment System for an Optical Cavity by Machine Learning	39
21	Akira Kawai	The University of Tokyo	Department of Physics	Single-pixel hyperspectral imaging for remote gas sensing	40
22	Yurina Michine	University of Electro-Communications	Institute for Laser Science	Stable and high damage threshold gas grating for ultra-high power laser system	41

Achieving High Efficiency in Solution-Processed Perovskite Solar Cells using C_{60}/C_{70} Mixed Fullerenes

Hao-Sheng Lin, Il Jeon, Yutaka Matsuo, Shigeo Maruyama
Department of Mechanical Engineering, The University of Tokyo, Tokyo 113-8656, Japan
linhaosheng@photon.t.u-tokyo.ac.jp

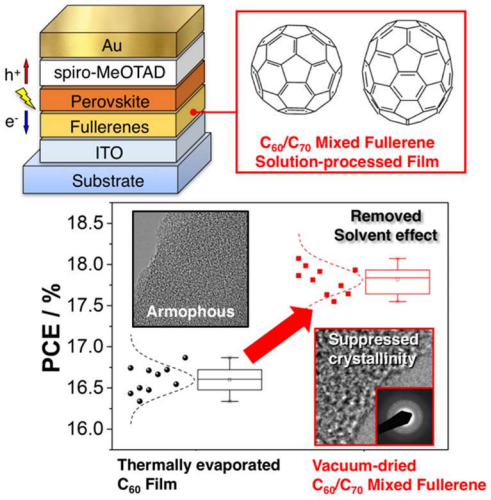

Fullerenes have attracted considerable interest as an electron transporting layer in perovskite solar cells. Fullerene-based perovskite solar cells produce no hysteresis and do not require high-temperature annealing. However, high power conversion efficiency can only be achieved when the fullerene layer is thermally evaporated, which is an expensive process. In this work,[1] the limitations of a solution-processed fullerene layer have been identified as high crystallinity and the presence of remnant solvents, in contrast to a thermally deposited C_{60} film, which has low crystallinity and no remaining solvents. As a solution to these problems, a mixed C_{60} and C_{70} solution-processed film, which exhibits low crystallinity, is proposed as an electron transporting layer. The mixed-fullerene-based devices produce power conversion efficiencies as high as that of the thermally evaporated C_{60}-based device (16.7%), owing to improved fill factor and open-circuit voltage. In addition, by vacuum-drying the mixed fullerene film, the power conversion efficiency of the solution-processed perovskite solar cells is further improved to 18.0%. This improvement originates from the enhanced transmittance and charge transport by removing the solvent effect. This simple and low-cost method can be easily used in any type of solar cells with fullerene as the electron transporting layer.

Reference:

1. Lin, H.-S.; Jeon, I.; Xiang, R.; Seo, S.; Lee, J.-W.; Li, C.; Pal, A.; Manzhos, S.; Goorsky, M. S.; Yang, Y.; Maruyama, S.; Matsuo, Y. *ACS Appl. Mater. Interfaces* **2018**, *10*, 39590-39598. (Selected as a journal cover)

Stable and Reproducible 2D/3D Formamidinium–Lead–Iodide Perovskite Solar Cells

Abhishek Thote, Il Jeon*, Shigeo Maruyama*, Yutaka Matsuo*, Hirofumi Daiguji*
Department of Mechanical Engineering, School of Engineering, The University of Tokyo, Japan
abhishekthote@thml.t.u-tokyo.ac.jp

2D perovskite-stabilized $FACsPbI_3$ (FA = Formamidinium) perovskite solar cells were fabricated in normal-type and inverted-type architectures. While the normal-type devices exhibited a high-power conversion efficiency of 20.2%, their reproducibility was limited. On the other hand, the inverted-type devices exhibited an efficiency of 18.2% with a greater stability and higher reproducibility than those of the normal-type devices. The reduced reproducibility of the normal-type devices was associated with the crack formation on the perovskite films during a spin-coating process. The hardness of both the perovskite and the sublayer was directly linked to the crack formation. Inverted-type 2D/3D $FACsPbI_3$ with ozone-treated poly(triarylamine) as sublayer exhibited high phase stability owning to the hydrophobic nature of poly(triarylamine) and improved energy level alignment upon an ozone-treatment. In addition, strong interaction between phenethylamine cations of the 2D perovskite and of the 3D $FACsPbI_3$ crystal at grain boundaries contributed to the high phase stability.

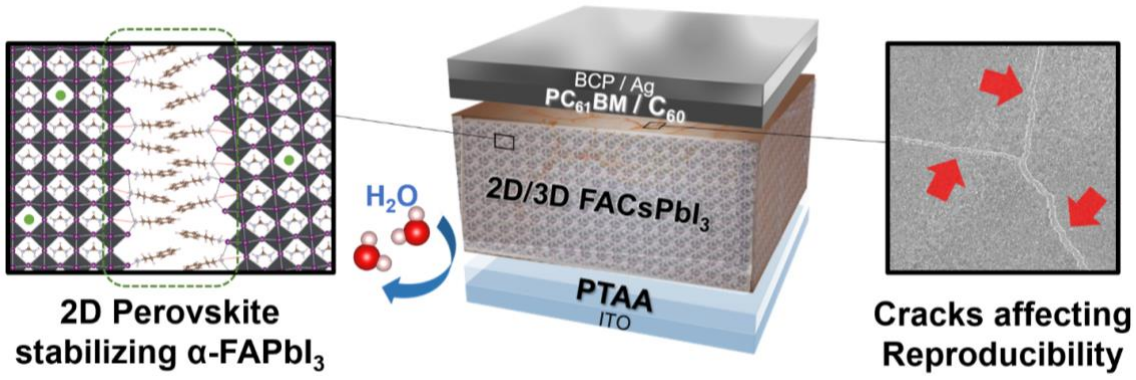

Figure 1: Illustration of molecular interactions in 2D/3D $FACsPbI_3$ (left), Inverted Perovskite Solar Cell device architecture (center) and SEM image of cracks on Perovskite films (right).

Growth of Boron Nitride Layers on Single-Walled Carbon Nanotubes and Graphite

○Hayato Arai[1], Satoshi Yotsumoto[1], Yongjia Zheng[1], Taiki Inoue[1], Rong Xiang[1], Shohei Chiashi[1], Shigeo Maruyama[1,2]

[1] *Department of Mechanical Engineering, The University of Tokyo, Tokyo 113-8656, Japan*
[2] *Energy Nanoengineering Lab, National Institute of Advanced Industrial Science and Technology (AIST), Ibaraki 305-8564, Japan*

Single-walled carbon nanotubes (SWCNTs) have been attracting attention since they were discovered. The excellent properties such as high carrier mobility [1] and high thermal conductivity [2] of SWCNTs make them promising material for nanoelectronics [3], optoelectronics [4], and so on. Hexagonal boron nitride (h-BN) and boron nitride nanotubes (BNNTs) also have been drawing interest as low-dimensional insulating materials. These materials can be used to screen the effects of impurities or substrates on the properties of graphene or SWCNTs [5, 6]. Therefore, synthesis of heterostructures of these materials are highly desired. We developed the facile CVD method to grow BN layers on SWCNT templates using ammonia borane as a precursor [7]. However, the detailed mechanism on nucleation and growth is still unclear.

In this work, we performed comparative study of BN-layer growth on SWCNTs and graphite for realizing higher quality SWCNT-BNNT heterostructures. Suspended SWCNTs and exfoliated graphite were prepared on Si substrates, and BN-layers were grown on them. The morphology of synthesized layers was investigated by SEM, TEM and AFM. As shown in Fig. 1(a), BN-layers were grown on SWCNTs. Figure 1(b) shows BN-layers grown on graphite surface. AFM observation reveals that BN-layers were grown to form pyramidal structures, which indicates the growth was non-self-limiting. Additionally, we compared BN-layers grown with and without hydrogen and found that hydrogen during CVD growth was effective for removal of the impurities which are derived from ammonia borane.

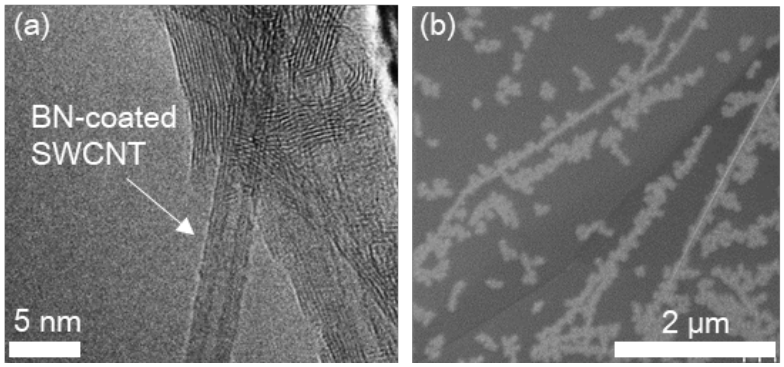

Fig. 1 (a) TEM image of BN-coated SWCNT. (b) SEM image of BN-layers grown on graphite surface.

[1] T. Durkop, *et al.*, *Nano Lett.*, **4**, 35 (2004).
[2] M. Fujii, *et al.*, *Phys. Rev. B*, **95**, 65502 (2005).
[3] S. J. Tans, *et al.*, *Nature*, **393**, 49 (1998).
[4] J. A. Misewich, *et al.*, *Science*, **300**, 783 (2003).
[5] C. R. Dean, *et al.*, *Nat. Nanotechnol.*, **5**, 722 (2010).
[6] A. Baumgartner, *et al.*, *Appl. Phys. Lett.*, **105**, 23111 (2014).
[7] R. Xiang, *et al.*, arXiv:1807.06154.

Enhancing the Stability of Perovskite Solar Cells via Lithium-ion Endohedral Fullerenes on Top of Laminated Carbon Nanotube Electrodes

○ Ahmed Shawky [1], Il Jeon [1], Hiroshi Ueno [2], Hiroshi Okada [1], Esko I. Kauppinen [3], Shigeo Maruyama,[1,4,*] and Yutaka Matsuo[1,2,*]

[1] Department of Mechanical Engineering, The Univ. of Tokyo, Tokyo 113-8656, Japan, [2] School of Chemistry, Northeast Normal Univ., Changchun, Jilin 130024, P. R. China, [3] School of Science, Aalto Univ. Aalto, FI-00076, Finland, [4] Energy Nano Engineering Lab., AIST, Ibaraki 305-8564, Japan

Replacing the metal electrode by carbon electrode has been reported to be one of the most effective ways in perovskite solar cell (PSC) technology toward commercialization. This aims to enhance the device stability of PSCs due to no ion migration and outstanding encapsulation effect. Among the carbon electrodes, the application of freestanding carbon nanotubes (CNTs) has given the highest PCEs with the use of 2,2′,7,7′-tetrakis(*N,N*-di-*p*-methoxyphenylamine)-9,9′-spirobi-fluorene (spiro-MeOTAD) hole transporting layer (HTL). However, it is reported that the use of Spiro-MeOTAD with hygroscopic lithium bis(trifluoromethanesulfonyl)imide (Li^+TFSI^-) limits the full potential of the CNT-PSCs in terms of long-term stability due to moisture-driven degradation. Recently, we reported lithium-ion-containing C_{60} fullerene trifluoromethanesulfonylimide salt ($[Li^+@C_{60}]TFSI^-$) that induced an instant oxidation of spiro-MeOTAD producing spiro-MeOTAD$^{\bullet+}TFSI^-$ and neutral $[Li^+@C_{60}]^{\bullet-}$ (= $Li@C_{60}$), which functioned as an antioxidant, protecting PSCs from intruding oxygen [1]. The stability of PSCs improved by 10-fold compared with the reference devices. Thus, combining the two technologies described above can provide a synergic and ultimate solution to the PSC stability.

Therefore, we incorporated the mixture of spiro-MeOTAD and $[Li^+@C_{60}]TFSI^-$ into the CNT top electrode in PSCs. The HTL solution is typically drop-casted onto the CNT network in CNT-PSCs. A saturated solution seeped through the CNT network while any undissolved $[Li^+@C_{60}]TFSI^-$ and $Li@C_{60}$ suspensions stayed on the top. This led to more effective hole extraction by avoiding $[Li^+@C_{60}]TFSI^-$ in the pathway and more effective anti-oxidation activity by placing $Li@C_{60}$ next to air. Since the drop-casting on CNTs separated the dissolved species from the undissolved species, the oxidation reaction of spiro-MeOTAD came to a stop. From various analyses and investigation, we found that 2 h stirring for the HTL solution gave the highest Photoconversion efficiency (PCE) of 17% and the longest operating stability of unencapsulated devices. The obtained PCE are close to the gold electrode-based PSCs (18.5%) while the device stability is approximately 100 times greater. Such excellent stability is attributed to no ion-migration and antioxidant activity of $Li@C_{60}$ that uniformly covering the CNT electrode. Not only did we demonstrate highly stable and efficiency CNT-PSCs but also discovered a new reaction mechanism within the spiro-MeOTAD and $[Li^+@C_{60}]TFSI^-$ HTL solution.

References:

[1] Jeon, I. *et al. Angew. Chemie Int. Ed.* **57,** 4607–4611 (2018).

Corresponding authors: maruyama@photon.t.u-tokyo.ac.jp, matsuo@photon.t.u-tokyo.ac.jp

Oil-in-water droplet formation in hydrophobic PDMS device using three-dimensional protruded taper channel

Dong Hyun Yoon, Tetsushi Sekiguchi, Shuichi Shoji
Faculty of Science and Engineering, Waseda University
yoon@shoji.comm.waseda.ac.jp

This research presents an oil-in-water droplet formation method of a liquid highly wetting on channel surface using three-dimensional structure. The three-dimensional structure allowed the droplet generation without hydrophilic treatment using structural feature only. The junction shape suppressed undesirable contact and spreading of oil on the wall surface. The strong contact and wide spreading of liquid on the surface is critical problem of droplet formation for unfavorable wetting condition.

The functional structure was fabricated by multi-layer stacking of PDMS structures. Four PDMS layers of six-layer fluidic channels were stacked for the three-dimensional and protruded structure. Diameters of droplets formed under various flow conditions and an effect of the channel morphology on the droplet formation results were evaluated. The results verified utility of the structure what we proposed for the droplet formation and the structure can be used as an element for droplet based research with various materials.

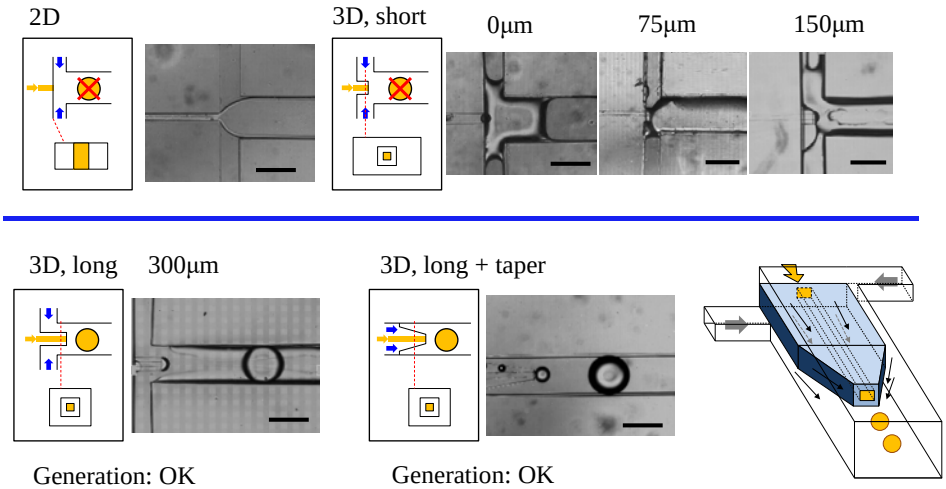

Figure 1. Effect of junction structure on droplet formation of highly wetting liquid and conditional limitation of the droplet formation.

Enhanced in-plane thermal conductivity of single-walled carbon nanotube/boron nitride nanotube composite films

P. Wang, Y. Zheng, T. Inoue, R. Xiang, M. Watanabe, S. Chiashi, S. Maruyama
Mechanical Engineering, School of Engineering, the University of Tokyo
wangpyk@photon.t.u-tokyo.ac.jp

Single-walled carbon nanotube (SWCNT) films exhibit promising potential as thermal interface material due to the superior thermal conductivity [1] and the outstanding mechanical property. However, it is still not yet successful for the SWCNT films to inherit the excellent thermal conductivity of ideal SWCNTs due to the limited thermal transport channels and relatively low oxidation temperature (450 500 ℃) [2,3]. Meanwhile, boron nitride nanotubes (BNNTs) possess high thermal conductivity comparable to SWCNTs and higher thermal stability in air than SWCNTs. A study has realized a 90% increase in thermal conductivity by encapsulating multi-walled CNT array with BNNTs [4].

In this work, we synthesized coaxial SWCNT-BNNT composite films by CVD method [5] and investigated thermal conductivity of them. FTIR spectra of the SWCNT films before and after coating with BNNTs are shown in Figure 1. In-plane thermal conductivity of this composite was studied by a contact free steady-state IR method [6] as schematically shown in Figure 2. We observed a thermal conductivity enhancement of SWCNT films (from ~68.1 W/m K to ~ 91.3 W/m K, ~ 30% increase) by further growing outer BNNTs (~3 walls). The characterization of the sample with SEM and TEM and the detailed experiment process will be presented.

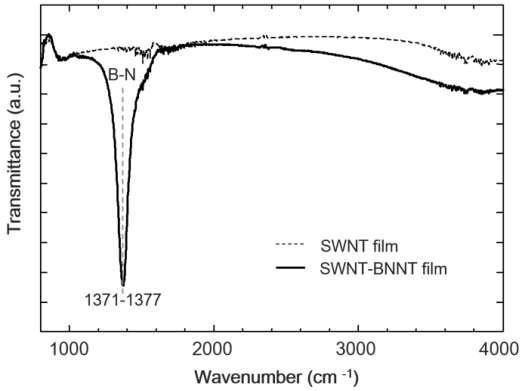

Fig. 1. Transmittance measured by FTIR of the SWCNT film and SWCNT-BNNT film.

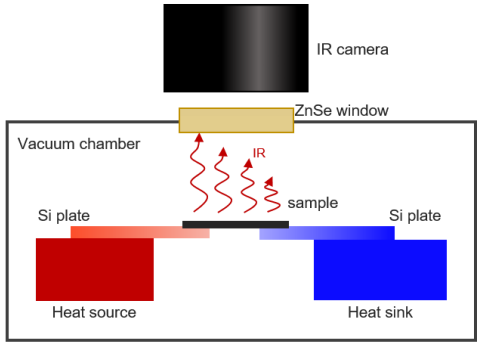

Fig. 2. A schematic of the thermal conductivity measurement setup.

[1] J. Hone *et al.*, Appl. Phys. Lett, **77**, 666 (2000). [2] A. M. Marconnet *et al.*, Rev. Mod. Phys., **85**, 3 (2013). [3] Y Chen *et al.*, Appl. Phys. Lett.**, 85**, 2430 (2004) [4] J. Lin *et al.*, ACS Appl. Mater. Interfaces, **9**, 14555 (2017). [5] R. Xiang *et al.*, arXiv :1807.06154 . [6] Y. Feng *et al.*, Jpn. J. Appl. Phys. **57** , 075101 (2018).

Isotope Labelling Analysis for Regrowth of Single-Walled Carbon Nanotubes

Bunsho Koyano[1], Shun Yamamoto[1], Keigo Otsuka[2,3], Taiki Inoue[1], Rong Xiang[1], Shohei Chiashi[1], Shigeo Maruyama[1,4]
[1]Department of Mechanical Engineering, The University of Tokyo
[2]Quantum Optoelectronics Research Team, Riken Center for Advanced Photonics
[3]Nanoscale Quantum Photonics Laboratory, Riken Cluster for Pioneering Research
[4]Energy NanoEngineering Lab, National Institute of Advanced Industrial Science and Technology (AIST)
koyano@photon.t.u-tokyo.ac.jp, yamamoto@photon.t.u-tokyo.ac.jp, keigo.otsuka@riken.jp, inoue@photon.t.u-tokyo.ac.jp, xiangrong@photon.t.u-tokyo.ac.jp, chiashi@photon.t.u-tokyo.ac.jp, maruyama@photon.t.u-tokyo.ac.jp

Single-walled carbon nanotubes (SWCNTs) are carbon materials whose diameter is about 1-2 nm and expected to be applied to electronic devices. However, the mechanism of SWCNT growth remains unclear in many ways, which makes it difficult to synthesize dense and long SWCNTs applicable to practical electronic devices. To elucidate the growth mechanism, we proposed a method for tracing the growth profiles of individual SWCNTs by embedding digitally coded isotope labels.[1] This method confirmed that SWCNTs followed the root growth mechanism in our condition. In this work, we investigated regrowth of SWCNTs after a pause of precursor gas and tried to find a method of reactivating SWCNTs. We introduced ^{13}C ethanol pulses with three different ratios while introducing ^{12}C ethanol. Ethanol was intentionally stopped for six minutes as an interval and introduced again after that (Fig. 1(a)). While ethanol was stopped, we introduced Ar, Ar/H_2, or water vapor and examined the change in SWCNT growth before and after the interval. Raman mapping was used to analyze G-band downshifts of individual SWCNTs (Fig. 1(b)). In the case of introducing Ar, no SWCNTs restarted growth after the interval. In the case of Ar/H_2, some SWCNTs show regrowth after the interval, and the growth rates are almost the same before and after the interval. However, in the case of water vapor, SWCNTs were etched toward their root parts during the interval and restarted growth after that, and the growth rates were generally higher after the interval than before (Fig. 1(c)). It is expected to synthesize highly dense and long SWCNTs by positive effects of water vapor on SWCNT growth.

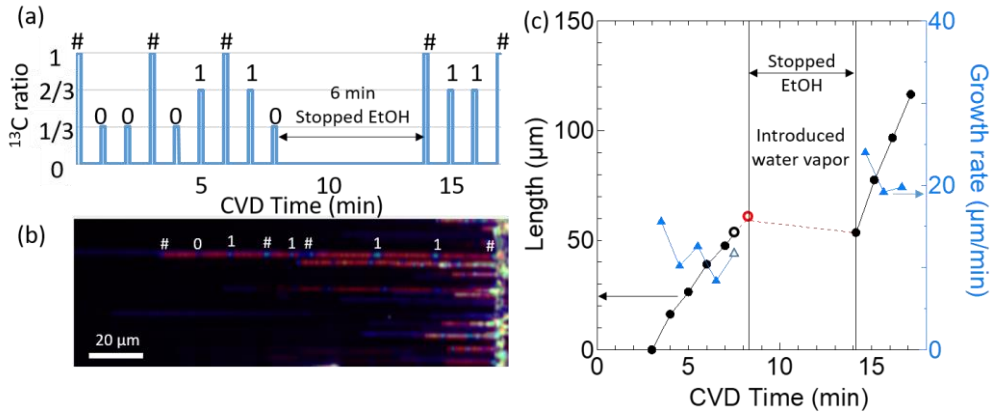

Fig. 1 (a) Example of introduction of ^{13}C ethanol labels. (b) Raman mapping image colored by the G-band shifts. (c) Growth curves of a SWCNT in the case of water vapor during the interval.
[1] K. Otsuka et al., ACS Nano 12, 3994 (2018).

Dynamical control of phase-change material coated Janus particles

R. Soma [1)], E. Yamamoto [1)], M. Kuwahara [2)], and T. Saiki [1)]

[1)] Graduate School of Science and Technology, Keio University, 3-14-1 Hiyoshi, Kohoku, Yokohama, Kanagawa 223-8522, Japan

[2)] National Institute of Advanced Industrial Science and Technology

ryo.soma@saiki.elec.keio.ac.jp

Colloidal particles in suspension are widely used for modeling of crystals and glasses to directly investigate the atomic-scale kinetics of phase transitions under optical microscope observation. Recently, active colloidal particles with self-propulsion capability attract more considerable attentions because they can mimic nonequilibrium dynamical system in nature. More importantly, self-propelled particles enable active delivery of cargo to the targeted site as required. Janus particles (JPs) are one of the active colloidal particles which are formed by two different hemispheres, whose physical/chemical properties are distinct from each other. The asymmetric feature of JPs provides self-propelled active motion.

In this study, we demonstrate self-propelled motion of silica microparticles partially coated with a phase-change switching material (Ge2Sb2Te5; GST) under application of AC electric field. GST is a material that can reversibly change between crystalline and amorphous phases and their dielectric properties are significantly different. Figure 1 shows sequential snapshots of self-propelling motion of JPs with their GST (amorphous) side facing forwards. Here, the AC voltage amplitude and frequency are 4.0 V and 2 kHz, respectively. We investigate the controllability of the swimming speed and direction with AC frequency and switching of the behaviors accompanying the phase change of GST. We found that the speed and direction of motion was successfully controlled by AC frequency and the phase of GST. The driving mechanism of self-propulsion is attributed to induced charge electro-osmosis.

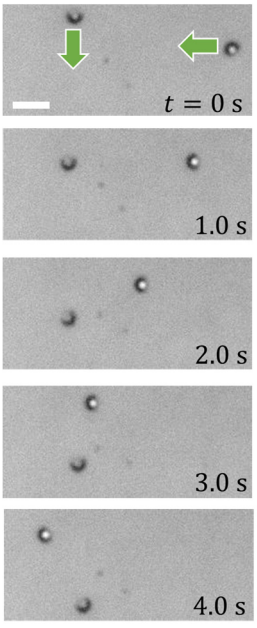

Fig. 1. Snapshots of self-propelling motion of JPs.

Dynamics of Colloidal Particles in a Temperature-Responsive Polymer Solution

B. Nakayama [1)], E. Yamamoto [1)], Y. Hiruta [1)], M. Kuwahara [2)], and T. Saiki [1)]

[1)] Graduate School of Science and Technology, Keio University, 3-14-1 Hiyoshi, Kohoku, Yokohama, Kanagawa 223-8522, Japan

[2)] National Institute of Advanced Industrial Science and Technology

bokusui.nakayama@saiki.elec.keio.ac.jp

Swarms of social insects, birds, or fish show quite reasonable behaviors, called 'swarm intelligence'. For examples, ants communicate among them via pheromone and they find the shortest path between their nest and food. Ants leave pheromone behind them in a round trip between nest and the food. Being attracted by the pheromone and tracking it, other ants can easily access the food. A variety of algorithms based on the swarm intelligence have been proposed and are widely utilized as a heuristic approach for combination optimization problem.

In this study, aiming to deeper understanding and new insights on the mechanisms of swarm intelligence, we propose an idea for physical implementation of ant colony optimization and demonstrated it experimentally. Individual agents are replaced by polystyrene beads (PBs) and a phase change material (GeSbTe) layer was used as a substrate, which is favorable for laser heating with a significant temperature gradient. We employed temperature-responsive polymer (Pluronic F127). The polymer in the vicinity of heated area turns to the sol state and PBs experience low viscosity and become mobile. The transition to the sol state acts as the signal left on the shared platform to communicate with other PBs. Figure 1 shows snapshots of microscope observation of motion of PBs accompanying gel-to-sol transition of F127 polymer, which is equivalent to the pheromone deposition. We observed chasing motion of particles, pheromone enhancement, thermal communication, and eventually formation of shortcut path.

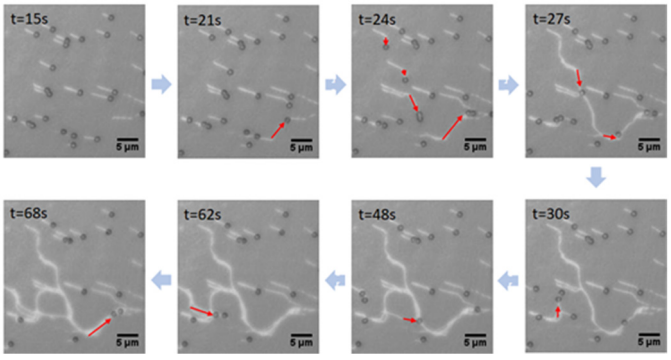

Fig. 1. Snapshots of microscope observation of motion of PBs.

Polyaromatic Anthracene Clencher on Single-Walled Carbon Nanotubes as Cathodes in Perovskite Solar Cells

○Shuhei Okawa[1], Il Jeon[1], Esko I. Kauppinen[2], Yutaka Matsuo[1], Shigeo Maruyama[1,3]

[1]*Department of Mechanical Engineering, The University of Tokyo, Tokyo 113-8656, Japan*

[2]*Department of Applied Physics, Aalto University School of Science, FI-00076 Aalto, Finland*

[3]*Energy Nano Engineering Laboratory, National Institute of Advanced Industrial Science and Technology (AIST), Tsukuba 305-8564, Japan*

okawa@photon.t.u-tokyo.ac.jp

Single-walled carbon nanotubes (SWNTs) possess excellent electrical conductivity and optical transparency, qualifying them for an alternative to transparent conductors in optoelectronic devices. SWNTs have been frequently used as an anode (hole-conductor) in perovskite solar cells (PSCs) [1] since SWNTs are naturally a p-type conductor in air. On the other hand, due to the low power conversion efficiency (PCE) arising from the challenging nature of its energy alignment, SWNT cathode has not been explored extensively. Previously, Jeon et al. reported a PCE of 10.5% from an inverted-type PSC in which a SWNT cathode drenched in $PC_{61}BM$ was used as the top electrode [2]. This demonstrated that the SWNT films can be used as a cathode and produce a PCE comparable to the anode counterpart.

In this work, we explored different materials to $PC_{61}BM$ to improve the SWNT cathode properties in PSCs from the optoelectronic perspective. After a through interface engineering of SWNTs cathodes, we achieved a PCE of 11.1% with SWNT film top electrode-based PSCs by incorporating polyaromatic anthracene ammonium (AA) molecules [3] which clenched onto SWNTs film [4] to enhance its charge selectivity. In order to protect perovskite layer from AA and ethanol, perovskite crystal was fully covered with $PC_{61}BM$ (Fig. 1 and 2). The resulting PSCs exhibited much higher PCE while being semi-transparent owing to AA firmly clenching onto the SWNTs and possessing a better energy alignment than $PC_{61}BM$.

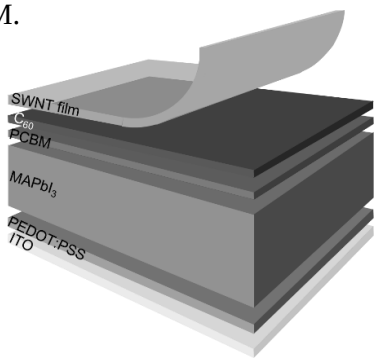

Fig. 1 Structure of the device.

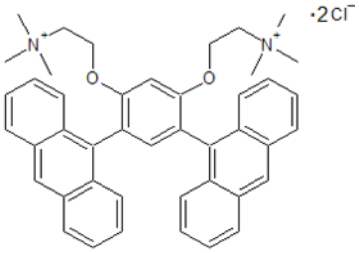

Fig. 2 Molecular structure of AA.

[1] Z. Li *et al*., *ACS Nano* **2014**, *8*, 6797.
[2] I. Jeon *et al*., *J. Phys. Chem. C* **2017**, *121*, 25743.
[3] I. Jeon *et al*., *ACS Appl. Mater. Interfaces* **2016**, 8, 29866.
[4] A. Kaskela *et al*., *Nano Lett.* **2010**, *10*, 4349.

Corresponding Author: S. Maruyama
Tel: +81-3-5841-6421,
Fax: +81-3-5800-6983,
E-mail: maruyama@photon.t.u-tokyo.ac.jp

Quantitative prediction of oxygen diffusion resistance and porous characters under capillary condensation of water in the mesoporous cathode catalyst layer of polymer electrolyte fuel cell

Toshihiro Kaneko[1*], Yuta Yoshimoto[1], Takuma Hori[2], Shu Takagi[1], Ikuya Kinefuchi[1]

[1] Department of Mechanical Engineering, The University of Tokyo

[2] Department of Mechanical Engineering, Tokyo University of Science

*Email: tkaneko@fel.t.u-tokyo.ac.jp (presenting author)

In the mesoporous cathode catalyst layer of polymer electrolyte fuel cell, water arises as the electrical power generation process goes on through $O_2 + 4H^+ + 4e^- \rightarrow 2H_2O$. It is known that the generated water fills the catalyst layer through capillary condensation that results in a reduction of power generation performance due to a significant increase in the oxygen diffusion resistance, but little is known about the quantitative relation among the oxygen diffusion resistance, the mesoporous characters and the amount of condensed water. An effective porosity and tortuosity factor are important parameters to characterize porous structures. In the case of the cathode catalyst layer, the effective porosity changes through capillary condensation of water and this effect must be considered appropriately. Our group developed coupled analysis simulation of lattice density functional theory and gas transport simulation of Knudsen flow region and applied to the porous media composed of randomly packed spheres [1]. In this work, we applied this approach for the actual structure of the mesoporous cathode catalyst layer obtained by a focused ion beam scanning electron microscope. First, the mesoporous cathode catalyst layer surrounded by bulk region is expressed as voxel data and the capillary condensation process of water is simulated by lattice density functional theory. Second, the oxygen diffusivity and the porous characters are calculated and the tortuosity factor is obtained. The calculated tortuosity factor, which is relevant to the oxygen diffusion resistance, is summarized as a function of effective porosity and they are compared to the Bruggeman equation [2].

References

[1] Y. Yoshimoto, T. Hori, I. Kinefuchi, and S. Takagi, *Phys. Rev. E* **96**, 043112 (2017).

[2] B. Tjaden, S. J Cooper, D. J. L. Brett, D. Kramer, and P. R. Shearing, *Current Opinion in Chemical Engineering* **12**, 44–51 (2016).

MOFA system at around 810 nm with Tm^{3+}-doped ZBLAN fiber

Eiji Kajikawa, Takashi Kubo, Tomohiro Ishii, Mitsuru Musha
Institute for Laser Science, Univ. of Electro-Communications
e_kajikawa@ils.uec.ac.jp

Fiber-based laser systems have advantages of compactness, high beam quality and robustness. Such a robust laser system at 813 nm is desired for the lattice laser of Sr optical lattice clock. The requirements of the lattice laser are the wavelength of 813.42 nm, the output power of more than 1 W, the linewidth of narrower than 1 MHz and single-transverse and longitudinal mode with continuous-wave. Among rare-earth ions, only Tm^{3+} has emission at around 810 nm. However the upper-state lifetime of Tm^{3+}-doped standard silica fibers are too short to amplify at the emission band due to its high phonon energy. Changing the host material from silica fibers to ZBLAN fibers, the upper-state lifetime is significantly increased up to 1.35 ms which is enough to amplify at the 810 nm band [1]. We have developed the master power fiber power amplifier (MOFA) system with Tm^{3+}-doped ZBLAN fiber. By using dual-wavelength pumping by Yb-fiber laser at 1050 nm and Raman fiber laser at 1220 nm and real-time photobleaching at 532 nm, we have obtained the maximum output power of 1.95 W with 5000 ppm Tm^{3+}-doped ZBLAN fiber, that is the highest output power at around 810 nm in fiber-based laser systems. Moreover, by applying the single-wavelength pumping at 1050 nm and real-time photobleaching with 15000 ppm Tm^{3+}-doped ZBLAN fiber, we have obtained the same slope efficiency as the dual-wavelength-pumped 5000 ppm Tm^{3+}-doped ZBLAN fiber. Our MOFA system would pave the way to realize the space Sr optical lattice clock.

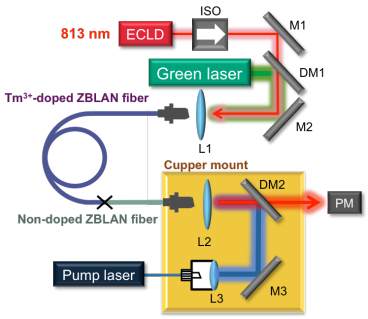

Fig. 1 Experimental setup

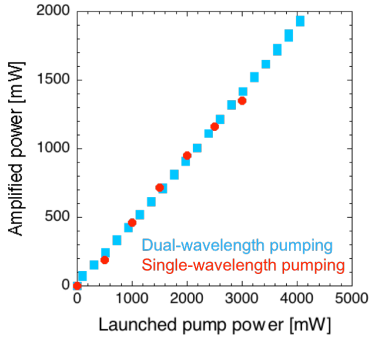

Fig. 2 Amplified power evolution

[1] Pavel Peterka, Ivan Kasik, Anirban Dhar, Bernard Dussardier, and Wilfried Blanc, Opt. Exp. **19,** 2773 (2011).

Coherent polarization beam combination for the light source of KAGRA

Rei Sakakibara
Department of Applied Physics, the University of Tokyo
sakakibara@g-munu.t.u-tokyo.ac.jp

KAGRA, the second-generation interferometric gravitational-wave detector in Japan, requires a high-power and high-quality (single mode oscillation, single frequency oscillation, low noises) laser to achieve its aimed sensitivity. For obtaining a high-power laser beam, fiber laser amplifiers are promising for its high-quality beam characteristics. However, such fiber laser amplifiers have a certain upper limit concerning their output power because nonlinear effects of optical fibers become significant and degrade the beam quality. Coherent beam combination (CBC) is one of the methods to overcome the power limitations of the fiber laser amplifiers.

There are several methods for CBC. One of them uses a beam splitter to combine two input beams with controlling relative phase between these beams. In this method, the reflectance and transmittance of the beam splitter should be determined taking account of the power ratio of two input beams. We are focusing on another method, called Coherent polarization beam combination (CPBC) where a polarizing beam splitter (PBS) is used to combine the laser beams; it can combine two beams with an arbitrary power ratio. Here, the power of two input beams (S-polarized and P-polarized beams) are combined without controlling relative phase, while the polarization state of the output beam is changed according to their relative phase. Thus, we also have to control the relative phase in CPBC.

In an ordinary system, to control the relative phase method, the input beams are phase-modulated by an electro-optic modulator. However, the modulation of the input beams can increase noises of the output beam. In order to realize low noises, we have developed a new method without any modulation of the beams. In this method, we only use a PBS, a quarter wave plate and a balanced photo-detector. We will present the principle of the new method and the details of the experimental system.

Water-Electrokinetic Energy Harvester using Flexible Woody Carbon Film

Seren Maeda[1], Hiroyuki Kuwae[1], Shuichi Shoji[1], and Jun Mizuno[2]

[1]School of Fundamental Science and Engineering, Waseda University

[2]Research Organization for Nano & Life Innovation, Waseda University

maeda@shoji.comm.waseda.ac.jp

Nowadays, energy harvesters using electrokinetic phenomena have attracted attention for internet of things (IoT) society [1]. Liquid or gas fluid flow inside the nano/microstructures induce electrical output called streaming current/voltage. However, the conventional devices are required complex fabrication process for realizing nano/microstructure. Here, we proposed a water-electrokinetic energy harvester using a flexible woody carbon film (FWCF). The concept of the proposed device is shown in Fig. 1. The FWCF is a flexible material with maintaining nano/microstructures of natural wood. Utilizing natural microchannels called tracheids, the device does not require complex fabrication process. The output performance of the fabricated device was characterized with not only deionized water-vapor flow and breathing, but also thermal-water evaporation flow.

The fabricated device showed a streaming voltage of about 9.7 μV with water-vapor flow. Moreover, the output of the device were enhanced by thermal-evaporation flow. The maximum output voltage was 421.3 μV. Moreover, the maximum power density of 8.5 nW/cm^{-3} was achieved at 80 °C under the thermal-water evaporation flow. In addition, electrical output was confirmed just breathing to the device. These results indicate that the proposed FWCF based water-electrokinetic power generation device has a high potential in power sources for IoT society.

[1] R. Zhang, *et al.*, Adv. Mater. 2015, 27, 6482-6487.

[2] G. B. Xue, *et al.*, Nature Nanotechnology. 2017, 12, 317–321.

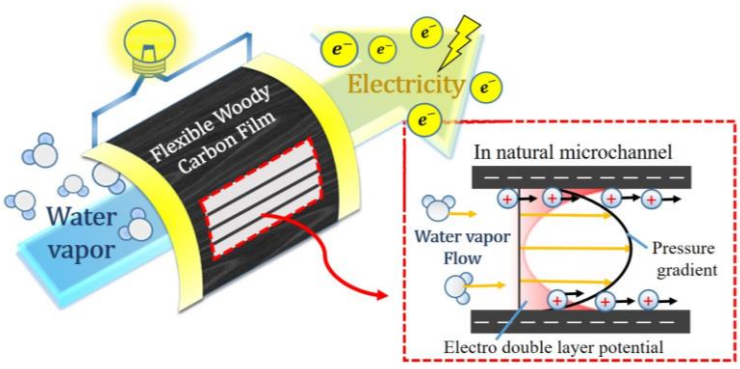

Fig. 1: Concept of the water-electrokinetic generation device using FWCF. Water vapor flow through the natural microchannels induces streaming current/voltage.

Energetics and electronic structure of single walled carbon nanotube encapsulated in boron nitride nanotube

○Kaoru Hisama[1], Susumu Okada[2], Shohei Chiashi[1] and Shigeo Maruyama[1,3]
[1] Department of Mechanical Engineering, The University of Tokyo, Tokyo 113-8656, Japan
[2]Graduate School of Pure and Applied Sciences, University of Tsukuba, Tsukuba 305-8571, Japan
[3] Energy NanoEngineering Lab., National Institute of Advanced Industrial Science and Technology (AIST), Ibaraki 305-8564, Japan,
Email: hisama@photon.t.u-tokyo.ac.jp

Tubular structures of C or BN allow them to form one-dimensional van der Waals (vdW) heterostructures by coaxially arranging them with appropriate diameter difference. Indeed, a recent experiment demonstrated that a carbon nanotube (CNT) is wrapped with BN nanotube (BNNT) [1] as an ultimate version of the surrounded gate transistor where CNT and BNNT are conducting channel and dielectric, respectively. Because the physical properties of CNT and BNNT are sensitive to their diameter, such one-dimensional vdW hybrids may exhibit interesting variation in their energetics and electronic structures, being different from the simple superpose of each constituent. Thus, in the present work, we aim to provide the energetics and electronic structures of CNT encapsulated in BNNT, using the density functional theory with the local density approximation.

Here, we consider double-walled NT consisting of inner (n,0) CNT and outer (m,0) BNNT, as the representative structure of the hybrids. The total energy calculation elucidated that the most stable combination of chirality index is m=n+9 where the interwall spacing is 0.35 nm. Under the optimum combinations, the calculated cohesive energies of the NTs are about 10 meV/atom weakly depending on the tube index and interwall atomic arrangements [Fig. 1(a)]. As for the electronic structure, band gaps of inner CNTs are modulated by forming the hybrid structures depending on the interwall stacking arrangements [Fig. 1(b)].

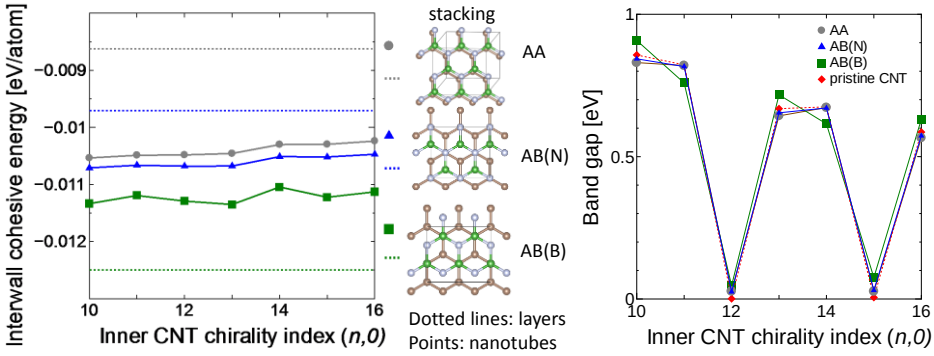

Figure 1 (a) Interwall cohesive energy and (b) band gap of CNT(*n*,0)@BNNT(*n*+9,0) as a function of the index *n*. Dotted lines in (a) indicate the cohesive energy of hBN and graphene with AB(B), AB(N) and AA stacking arrangements.

[1] R. Xiang, *et al.*, arXiv preprint arXiv:1807.06154.

(Notice: This talk includes as the same content as The 56th Fullerenes-Nanotubes-Graphene General Symposium, 2P-2, March 3rd (Sun.), 2019)

Gauge-Invariant Time-Dependent Configuration Interaction Singles Method for Multielectron Dynamics under Intense Laser Field

Takuma Teramura, Takeshi Sato, and Kenichi L. Ishikawa
Department of Nuclear Engineering and Management,
Graduate School of Engineering, The University of Tokyo
teramura@atto.t.u-tokyo.ac.jp

Chirped pulse amplification, awarded the Nobel prize in 2018, has enabled to generate intense laser pulses and opened up a new field of high-field physics. In this regime, various high-field phenomena such as high-harmonic generation (HHG) take place. Although electron dynamics triggered by external laser pulses is rigorously described by the time-dependent Schrödinger equation, direct numerical solution of the equation is unfeasible for most multielectron systems. Thus, various first-principles methods to describe multielectron dynamics have been developed.

Among them, time-dependent configuration interaction singles (TDCIS) method is a powerful approach. In this method, the total *N*-electron wavefunction $\Psi(r_1 \cdots r_N; t)$ is approximated by a linear combination of time-independent Slater determinants

$$\Psi(r_1 \cdots r_N; t) = \Phi_0(r_1 \cdots r_N) C_0(t) + \sum_i^{\mathrm{occ}} \sum_a^{\mathrm{vir}} \Phi_i^a(r_1 \cdots r_N) C_i^a(t),$$

where r_i is a position of the i-th electron, Φ_0 is the Hartree-Fock ground state, and Φ_i^a is a singly excited configuration replacing an occupied orbital ϕ_i with a virtual one ϕ_a. The electron dynamics is described by the evolution of CI coefficients (C_0 and $\{C_i^a\}$). Utility of the TDCIS method has been enhanced by reformulating the TDCIS method by using channel orbital defined by $\chi_i(r,t) = \sum_a^{\mathrm{vir}} \phi_a(r) C_i^a(t)$, which removes a computational bottleneck of calculating and storing huge number of virtual orbitals $\{\phi_a\}$ [1]. However, the conventional TDCIS method suffers from a violation of gauge-invariance, which prevents efficient simulations of high-field phenomena. In this contribution, we report gauge-invariant reformulation of the TDCIS method [2] and its successful implementation to three-dimensional atoms, including applications to HHG from He and Ne atoms.

References

[1] N. Rohringer, A. Gordon, and R. Santra, Phys. Rev. A 74, 043420 (2006).

[2] T. Sato, T. Teramura, and K. L. Ishikawa, Appl. Sci. 8, 433 (2018).

Low Cost and High-Efficient Piezoelectric MEMS Energy Harvester with Interdigitated Electrodes and Liquid-based VDF-TrFE

Kenta Sasagawa[1], D. H. Yoon[1], Tetsushi Sekiguchi[2],
Toshio Sasaki[2], Takashi Nakajima[3], and Shuichi Shoji[1]
[1] Waseda University, Tokyo, Japan,[2]Nanotechnology Research Center, Waseda University, Japan
[3]Tokyo University of Science, Tokyo, Japan
E-mail: sasagawa@shoji.comm.waseda.ac.jp

This paper reports a novel vibration-based MEMS scale energy harvester, which consists of Si interdigitated electrodes and polymeric piezoelectric material (VDF/TrFE). Low cost and high-efficient energy harvester was achieved by the high aspect ratio interdigitated electrode structure, which was simply fabricated by a single etching process. By taking advantage of liquid-based polymer, piezoelectric material is formed between interdigitated electrodes by simple spin coating. Output voltage of about 300 mV was obtained per impact force of 1 N.

Two types of device were fabricated: one is the device with glass as a substrate of electrodes and the other is the device without it. Fig.1 shows the photographs of the electrodes without glass as a substrate of electrodes. Silicon was etched to the bottom and interdigitated electrodes with height and gap of approximately 200 μm and 60 μm were successfully fabricated. Fig.2 shows the evaluation results of maximum peak to peak voltage when balls of different weight were dropped. As a result, output voltage of about 300 mV per impact force of 1 N was achieved with the device without glass.

Considering the simple fabrication process and the performance, the proposed device structure is applicable for low cost and high-performance energy harvesters.

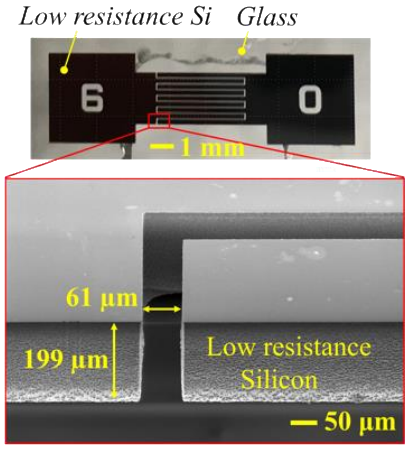

Fig. 1 Image of the interdigitated electrodes.

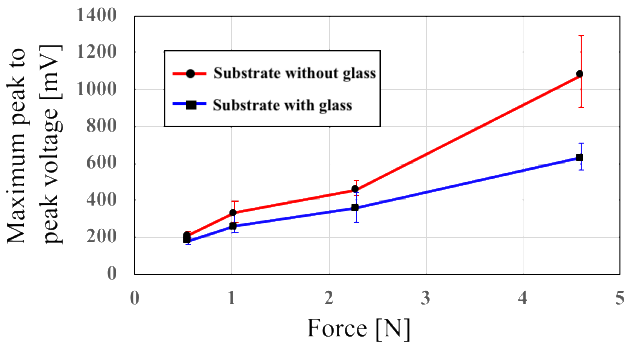

Fig.2 Maximum peak to peak voltage by different force.

Theoretical study on inter-atomic distance effects on high-order harmonic generation

Mizuki Tani[1], Yasushi Shinohara[2], Takeshi Sato[2], Kenichi L. Ishikawa[2]

1.*Faculty of Engineering, The Univ. Tokyo, Tokyo, Japan*

2.*School of Engineering, The Univ. Tokyo, Tokyo, Japan*

E-mail: forultraplayers1@g.ecc.u-tokyo.ac.jp

Spectral features of high-order harmonic generation (HHG) are quite different between the solid and the gas phases. While HHG in the gas phase is well understood by the three-step model [1], a comprehensive mechanism of solid-state HHG is still under active research [2-4]. To elucidate the origin of the difference, Hansen *et al.* [5,6] have studied the transition between the gas-phase and solid-state HHG in terms of the number of atoms and found a critical number of atoms where the harmonic spectrum starts to show a solid-like feature. In this study, we investigate the transition in terms of the inter-atomic distance (IAD).

We simulate HHG from one-dimensional model periodic systems by solving the time-dependent Schrödinger equation within the independent electron approximation. We use a local potential which has the ground-state level (~ -14 eV) comparable to that of the hydrogen atom. The IAD is included as distance between the periodically arranged potential wells and varied between 0.5 nm - 50 nm. We evaluate the time-dependent current density as the expectation value of induced velocity and the HHG spectrum as a power spectrum of the current density. The laser electric field is given by $E(t) = -\mathrm{d}A/\mathrm{d}t$, $A(t) = -(E_0/\omega)\sin^4(\pi t/T)\cos[\omega(t - T/2)]$, $T = 24.16$ fs, $\hbar\omega = 1.55$ eV, corresponding to 800 nm wavelength.

We have found that the HHG spectrum shows two transitions around small IAD (~ 0.7 nm) and large IAD ($\lesssim$ 50 nm). Our analyses show that, while the former is a static effect due to a change of electronic structure, the latter is a dynamic effect related with the electronic motion in the laser field.

[1] P. B. Corkum, Phys. Rev. Lett. 71 (1993) 1994

[2] K. Kaneshima, Y. Shinohara, K. Takeuchi, N. Ishii, K. Imasaka, T. Kaji, S. Ashihara, K. L. Ishikawa, and J. Itatani Phys. Rev. Lett. 120 (2018) 243903

[3] T. Ikemachi, Y. Shinohara, T. Sato, J. Yumoto, M. Kuwata-Gonokami, and K. L. Ishikawa. Phys. Rev. A 95 (2017) 043416

[4] T. Ikemachi, Y. Shinohara, T. Sato, J. Yumoto, M. Kuwata-Gonokami, and K. L. Ishikawa Phys. Rev. A 98 (2018) 023415

[5] K. K. Hansen, T. Deffge, and D. Bauer, Phys. Rev. A 96 (2017) 053418

[6] K. K. Hansen, D. Bauer, and L. B. Madsen, Phys. Rev. A 97 (2018) 043424

Molecular contrast added to phase-contrast microscope

Keiichiro Toda[1], Miu Tamamitsu[1], Ryoichi Horisaki[2,3], and Takuro Ideguchi[1,3]

1. Department of Physics, The University of Tokyo

2. Graduate School of Information Science and Technology, Osaka University

3. PRESTO, Japan Science and Technology Agency

toda@gono.phys.s.u-tokyo.ac.jp

Label-free imaging techniques provide solutions for non-invasive analysis of biological specimen. Raman scattering and Infrared absorption microscopes are often used for label-free molecular imaging, but these microscopes suffer from the low sensitivity or low spatial resolution, respectively .

Here, we propose and demonstrate a label-free molecular contrast (MC) imaging technique based on a standard phase-contrast (PC) microscope, called MC-PC microscope [Fig.1(a)], with high sensitivity and spatial resolution. Intensity modulated mid-infrared (MIR) light excitation induces modulated PC images due to the photothermal effect, which is visualized as a MC image. This microscope provides high sensitivity due to the MIR molecular absorption and high spatial resolution due to the PC imaging with visible light [1]. With the developed system, we show the capability of ultrafast molecular-image acquisition (3,000 frames per second, which is an order of magnitude higher than the state-of-the-art molecular imaging [2]) with microbeads, and broadband spectroscopic imaging with Henrietta Lacks (HeLa) cells [Fig. 1(b),(c),(d)].

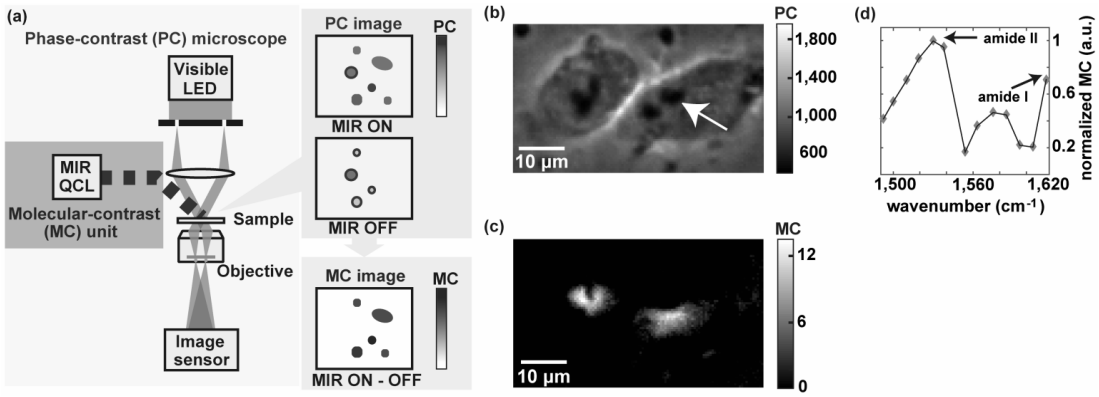

Fig. 1. MC-PC microscope. (a) Principle of MC-PC microscope. QCL: quantum cascade laser, LED: light-emitting diode. (b) PC image of HeLa cells. (c) MC image for 1,530 cm^{-1} excitation, which shows the intracellular protein distribution. (d) MC spectra obtained at the site indicated by the arrow in (b).

[1] K. Toda et al., arXiv: 1812.04576 (2018). [2] Y. Ozeki et al., Nat. Photonics **6**, 845 (2012).

Development of an Auto-Alignment System for an Optical Cavity by Machine Learning

Hiroyuki Tahara[1] and Norikatsu Mio[1,2]

[1]Department of Applied Physics, University of Tokyo

[2]Institute for Photon Science and Technology, University of Tokyo

tahara@g-munu.t.u-tokyo.ac.jp

Considering the current situation where the systematic and versatile methods for obtaining good alignment of an optical cavity hardly exist, we are developing an auto-alignment system for the cavity with a wide control range and a simple optical setup by making a good use of the computational resources. When the cavity is locked to TEM_{00} of an incident laser beam, its higher-order eigenmode components reflected off at an input mirror of the cavity contains information concerning misalignment. We designed a machine learning technique for extracting the misalignment information from reflected light. We adopted a supervised learning scheme for deep neural networks, of which the input data are intensity distributions of the reflected light ray observed at two positions; the outputs of the networks are used to predict the sign of each component of a gradient vector of transmission power expressed as function of four degrees of freedom in two alignment mirrors. Using the trained deep neural networks as shown in the flowchart below, we have accurately operated the auto-alignment system and made the alignment state as good as the best realized by the manual procedure.

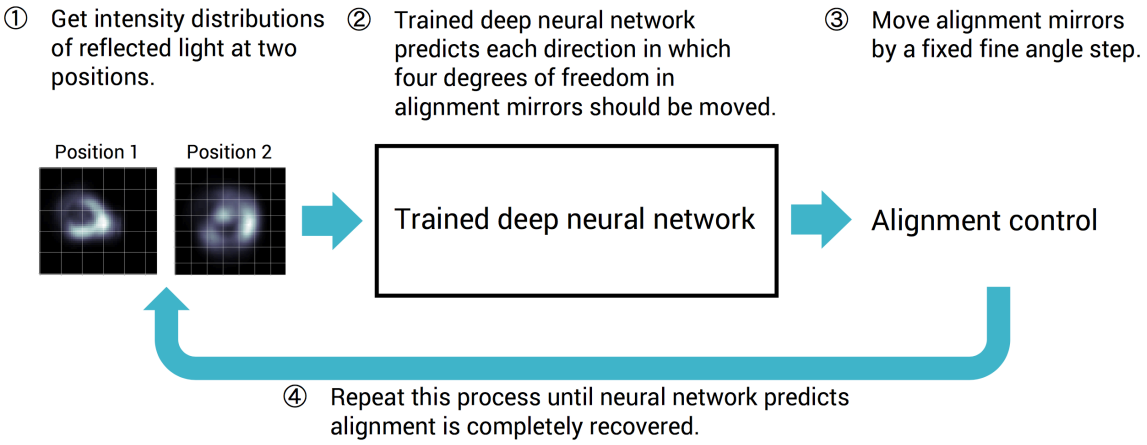

Single-pixel hyperspectral imaging for remote gas sensing

Akira Kawai[1], Yuki Yoshida[1], Kazuki Hashimoto[1,2], and Takuro Ideguchi[1,3]

1. *Department of Physics, The University of Tokyo*
2. *Aeronautical Technology Directorate, Japan Aerospace Exploration Agency*
3. *PRESTO, Japan Science and Technology Agency*

kawai@gono.phys.s.u-tokyo.ac.jp

Hyperspectral imaging is an established tool for solving chemical and biological problems in various fields such as environmental monitoring, clinical diagnosis, and food analysis [1]. However, its spectral bandwidth and resolution are limited by grating spectrometers employed in conventional hyperspectral cameras. Therefore, it has never been possible to take images of several molecular species in gas phase, because it requires broadband and high-resolution hyperspectral images.

Here, we propose and demonstrate broadband hyperspectral imaging that enables us to obtain gaseous absorption spectral images at line-resolved spectral resolution with a simple setup. It is made possible by combining single-pixel imaging and Fourier-transform spectroscopy (Fig. 1). To demonstrate the concept, we measure a hyperspectral image of gaseous HCN with a developed single-pixel Fourier-transform spectro-imaging system.

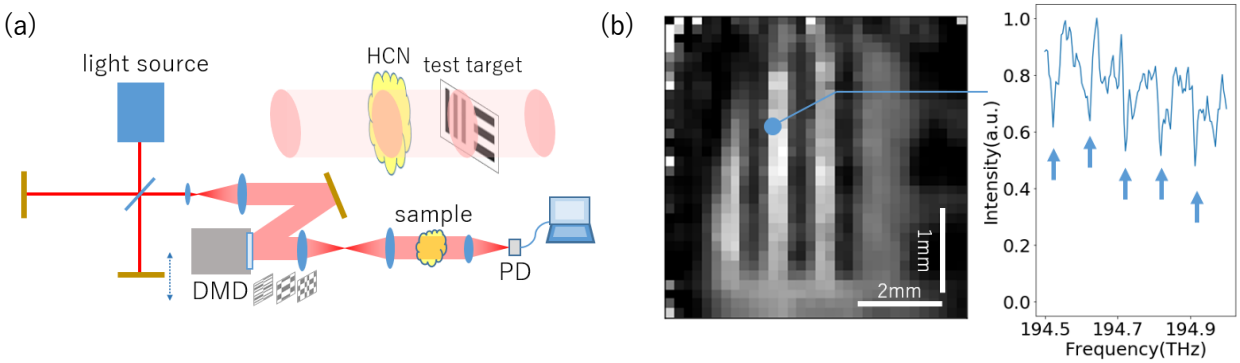

Fig. 1 (a) Schematic of the system. DMD: Digital Mirror Device. (b) Hyperspectral image of the test target together with HCN gas. The image is processed with bilateral filter.

[1] Jin, S., *et al*., Sci. Rep. **7,** 1-7 (2017).

[2] Hashimoto, K., and Ideguchi, T., Nat. Commun. **9,** 4448 (2018).

Stable and high damage threshold gas grating for ultra-high power laser system

Yurina Michine

Institute for Laser Science, University of Electro-Communications

y_michine@ils.uec.ac.jp

Recently required power and energy of laser systems are increased drastically. The maximum energy of nanosecond laser exceeded Mega(10^6) J and maximum power reached to Exa-watt (10^{18}) level. Even though such inflation of output laser performance, laser induced damage threshold of optics is still remained with several J/cm^2 levels. Therefore, high power laser system size increased year by year. However, some optics (for example, grating) are considered to be beyond present human technology limit. It is strong motivation to develop higher damage threshold optics. For this purpose, we propose ozone assisted gas grating for such high energy laser systems with ultra-high damage threshold.

Our new gas optics is created by UV laser (excimer laser, λ= 248nm, 20ns, 100mJ) and ozone mixed oxygen gas. Figure 1 shows schematic drawing of the grating. This system is consisted with atmospheric discharge part and UV writing area for high power laser diffraction. At the diffraction area, two beams of UV pulse laser interferer each other to make spatial modulation of refractive index in atmosphere. The third diffraction beam is entered to grating area and diffract.We archived 96% average diffraction efficiency with 70mJ/cm^2 UV laser energy. We already demonstrated (1) high damage threshold for ns lasers (1.7kJ/cm^2) (2) high average diffraction efficiency (<96%) (3) low production energy (<70mJ/cm^2). This grating will be used

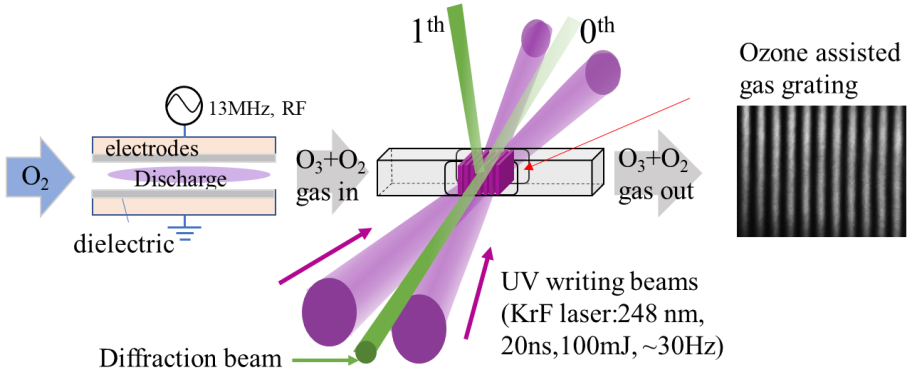

Figure 1. Configuration of ozone mixed gas grating

Appendix

FUKUTAKE HALL

Access

Approximate walking distances from the nearest stations:

- 7 mins from Hongo Sanchome Station on the Toei Subway Oedo Line
- 8 mins from Hongo Sanchome Station on the Tokyo Metro Marunouchi Line
- 20 mins from Yushima Station on the Tokyo Metro Chiyoda Line
- 10 mins from Todai Mae Station on the Tokyo Metro Nanboku Line

Opening Hours

Fukutake Hall is open from 8am to 8pm, Monday to Friday.

(It is also open at weekends when special events are being held.)

Contact Information

(Reception Desk)

Telephone	03-5841-0328
e-mail	fukutakehall@iii.u-tokyo.ac.jp

THE UNIVERSITY OF TOKYO

Access Map

○ Nearest Station (Walk or bus)

■ Junctions

See campus maps for bus/walking routes from nearest stations.

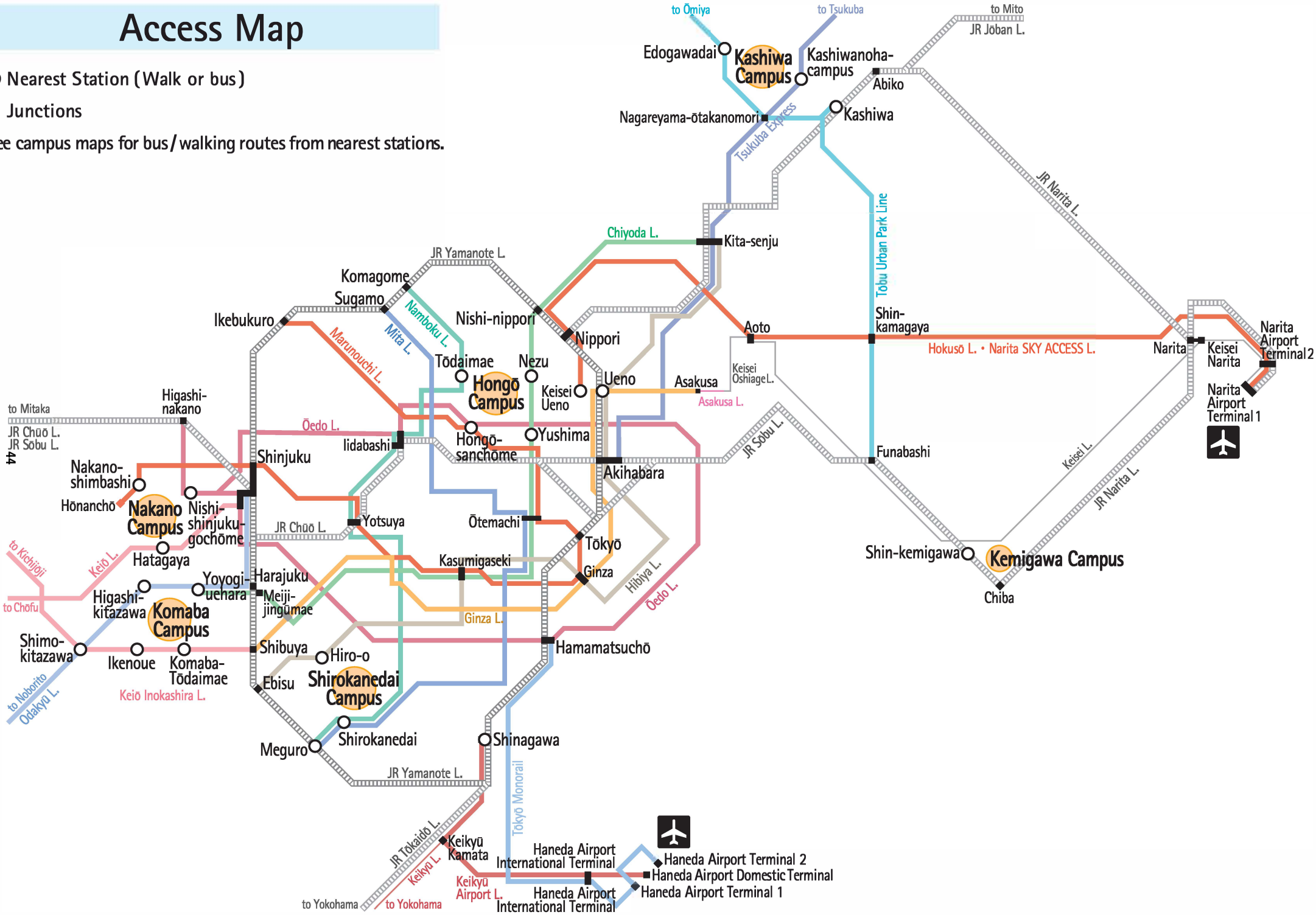

Hongō Campus

Getting to the Hongō Campus

- Hongō-sanchōme Station (Subway Marunouchi Line)
  8 minutes' walk.
- Hongō-sanchōme Station (Subway Ōedo Line)
  6 minutes' walk.
- Yushima Station or Nezu Station (Subway Chiyoda Line)
  8 minutes' walk.
- Todaimae Station (Subway Namboku Line)
  1 minute's walk.
- Kasuga Station (Subway Mita Line)
  10 minutes' walk.
- Ochanomizu Station (JR Chūo Line, JR Sōbu Line)
  <Subway>Subway Marunouchi Line (for Ikebukuro)
  → get off at Hongō-sanchōme Station.
  <Subway>Subway Chiyoda Line (for Toride)
  → get off at Yushima Station or Nezu Station.
  <Toei Bus>茶51 for Komagome Station South Exit or 東43 for Arakawa-dote-sōshajō
  → get off at Todai-Akamon-mae, Todai-Seimon-mae, Todai-Nōgakubu-mae stops
  <Toei Bus>学07 for the University of Tokyo
  → get off at Tatsuokamon, Todai-Byōin-mae, Todai-Kōnai stops.
- Ueno Station (JR Yamanote Line, other lines)
  <Toei Bus>学01 for the University of Tokyo
  → get off at Tatsuokamon, Todai-Byōin-mae, Todai-Kōnai stops.
- Okachimachi Station (JR Yamanote Line, other lines),
  <Toei Bus>都02 for Ōtsuka Station or 上69 for Otakibashi-shako-mae
  → get off at Yushima-yonchōme, Hongō-sanchōme Eki-mae stops.

1 Yasuda Auditorium
2 Sanjō Conference Hall
3 Ikutokuen (Sanshirō Pond)
4 Chūō Refectory (Underground)
5 Second Refectory
6 Administration Bureau
7 General Library
8 Shichitokudō (Japanese Sports Gymnasium)
9 Administration Bureau Bldg.2
International Center, Hongō Office・USTEP Office
Center for Japanese Language Education
Center for Research and Development of Higher Education
Graduate School of Public Policy
Hongō Health Service Center
Integrated Research System for Sustainability Science (IR3S)
10 Kaitokukan
11 Ikutokudō (Japanese Archery Range)
12 Student Counseling Center
Nandemo-Sodan (One-Stop Resources) Office
Communication Support Room
Peer Support Room
Career Support Office
13 Yayoi Auditorium
14 Yayoi Auditorium Annex
15 Information Center
16 Sanjō Conference Hall Tatsuokamon Annex
17 UCR Plaza
18 Gotenshita Athletic Field
19 Baseball ground
20 Athletic Field
21 Gotenshita Memorial Arena
Student Support Center
Disability Services Office
22 Communication Center
23 Overhead Bridge
24 Tennis Courts (Under Construction)
25 Tennis Courts
26 Tennis Courts
27 Entrepreneur Plaza
28 Mukougaoka Faculty House
29 Itō International Research Center
Itō Hall
Executive Management Program Office
Policy Alternatives Research Institute
30 Faculty of Law & Letters Bldg.1
31 Faculty of Law & Letters Bldg.2
32 Faculty of Law Bldg.3
33 Faculty of Law Bldg.4
34 General Research Bldg.
35 School of Law Bldg.
36 Faculty of Letters Bldg.3
37 Akamon General Research Bldg.
38 Faculty of Letters Annex
39 Economics Research Bldg.
40 Economics Research Annex (Kojima Hall)
41 Faculty of Education
42 Faculty of Medicine Bldg.1
Harassment Counseling Center
43 Faculty of Medicine Bldg.2
44 Medical Library
International Research Center for Medical Education
45 Faculty of Medicine Bldg.3
46 Faculty of Medicine Annex of Bldg.3
47 Bioscience Research Bldg.
48 Faculty of Medicine Bldg.4
49 Faculty of Medicine Bldg.5
50 Faculty of Medicine Experimental Research Bldg.
51 Faculty of Medicine International Research Center
52 Clinic
53 Ward A
54 Ward B
55 Central Bldg. (East Wing)
56 Central Bldg. (South Wing)
57 Central Clinical Service Bldg.1
58 Central Clinical Service Bldg.2
59 First Research Bldg.
60 East Clinical Research Bldg.
61 Molecular & Life Innovation Bldg.
62 Administration & Research Bldg.
63 Clinical Research Bldg.A
64 South Clinical Research Bldg.
65 Clinical Research Ward
60 Advanced Clinical Research Center
67 Energy Station
68 Faculty of Pharmaceutical Sciences
69 Pharmaceutical Sciences Research Bldg.
70 Pharmaceutical Sciences Library
71 Frontier Sciences for Drug Discovery Bldg.
72 Head Administration Office of Engineering (Reppinkan)
73 Faculty of Engineering Bldg.1
74 Faculty of Engineering Bldg.2
75 Faculty of Engineering Bldg.3
76 Faculty of Engineering Bldg.4
77 Faculty of Engineering Bldg.5
78 Faculty of Engineering Bldg.6
79 Faculty of Engineering Bldg.7
80 Faculty of Engineering Bldg.8
81 Faculty of Engineering Bldg.9
Institute of Engineering Innovation
82 Faculty of Engineering Bldg.10
83 Faculty of Engineering Bldg.11
84 Faculty of Engineering Bldg.12
85 Faculty of Engineering Bldg.12 Annex
86 Faculty of Engineering Bldg.13
87 Faculty of Engineering Bldg.14
88 Takeda Bldg.
Takeda Hall
VLSI Design and Education Center
89 Seakeeping Tank; Ship Model Basin
90 Experimental Tank
91 Cavitation Tunnel
92 Monozukuri Lab.
93 Power Dynamics Experiment Laboratory
94 Wind Engineering Lab.
95 High Voltage Electron Microscope
96 I-REF Bldg.
97 Faculty of Science Bldg.1 (East) (Under Construction)
98 Faculty of Science Bldg.1 (Center) Koshiba Hall
99 Faculty of Science Bldg.1 (West)
International Center for Elementary Particle Physics
100 Faculty of Science Bldg.2
101 Faculty of Science Bldg.3
102 Faculty of Science Bldg.4
103 Faculty of Science Bldg.7
104 Faculty of Science Chemistry Bldg.
105 Faculty of Agriculture Bldg.1
106 Faculty of Agriculture Bldg.2
107 Faculty of Agriculture Bldg.2 Annex
108 Faculty of Agriculture Bldg.3
Asian Natural Environmental Science Center
109 Faculty of Agriculture Bldg.5
110 Faculty of Agriculture Bldg.6
111 Faculty of Agriculture Bldg.7A
112 Faculty of Agriculture Bldg.7B
113 University Library for Agricultural and Life Sciences
114 Agricultural and Life Sciences Museum
115 Life Sciences Research Bldg.
116 Veterinary Medical Center
117 Biotechnology Research Center
118 Food Science Bldg.
119 Life Sciences Research Bldg.B
120 Protein Research Laboratory
121 Interfaculty Initiative in Information Studies & Graduate School of Interdisciplinary Information Studies
122 iii-Fukutake Hall
123 iii-Daiwa Ubiquitous Computing Research Bldg.
124 Earthquake Research Institute Bldg.1
125 Earthquake Research Institute Bldg.2
126 Earthquake Research Institute Bldg.3
127 Institute of Molecular and Cellular Biosciences
128 Institute for Advanced Studies on Asia
129 Institute of Social Science
130 Historiographical Institute
131 University Museum
132 Micro Analysis Laboratory, Tandem Accelerator (MALT)
133 Environmental Science Center
134 Environmental Science Center Annex
135 Isotope Science Center
136 Information Technology Center
137 Information Technology Center Annex
138 Cryogenic Research Center

2016.5

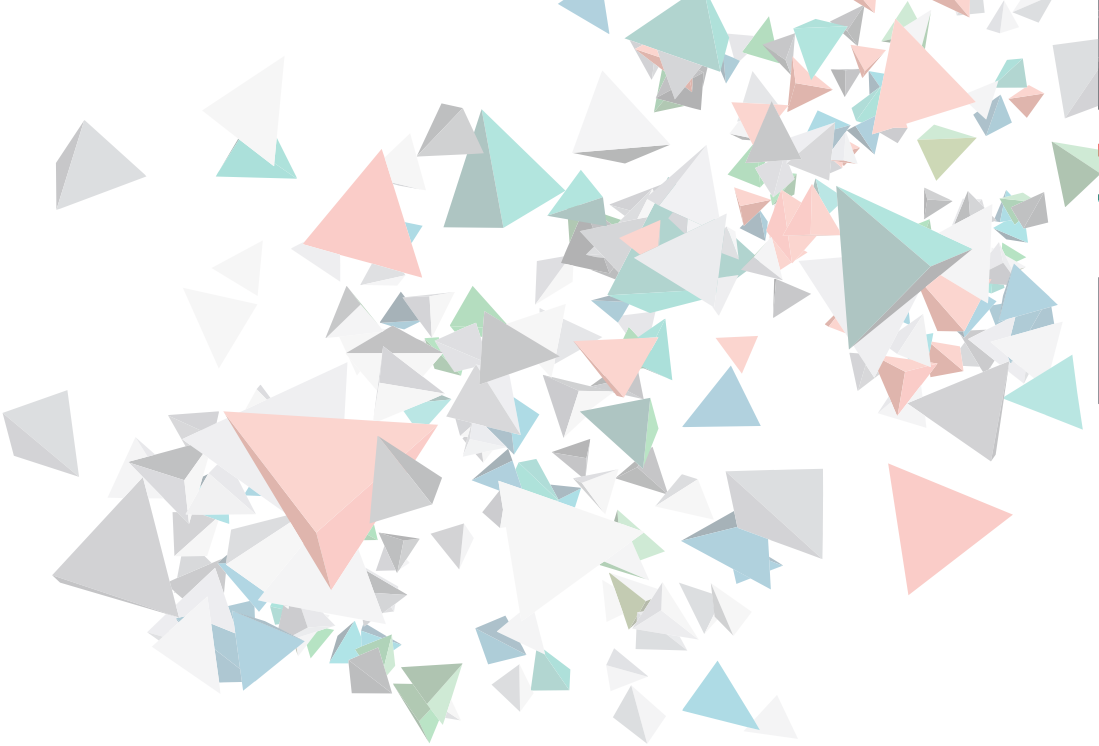

CIAiS

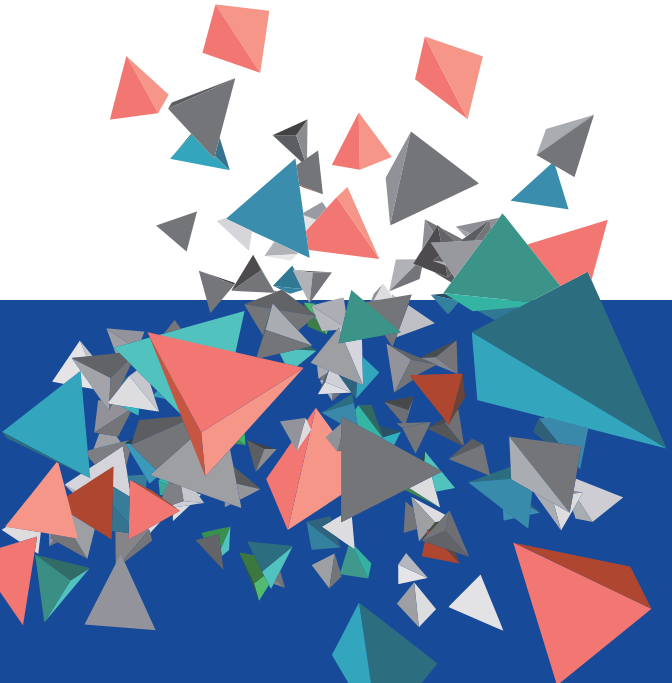

Research and Education Consortium for Innovation of Advanced Integrated Science

GMSI Office, The University of Tokyo
ENG.Bldg.2-203 7-3-1 Hongo, Bunkyo-Ku, Tokyo, 113-8656, Japan
TEL&FAX:03-5841-0696 Email:office@gmsi.t.u-tokyo.ac.jp
http://ciais.t.u-tokyo.ac.jp/